

# Phase Space Ray Tracing for Illumination Optics

Carmela Filosa

Cover art:  
Photography:

A catalogue record is available from the Eindhoven University of Technology Library

ISBN: 978-90-386-3972-7

Copyright © 2017 by C. Filosa.

All rights are reserved. No part of this publication may be reproduced, stored in a retrieval system, or transmitted, in any form or by any means, electronic, mechanical, photocopying, recording or otherwise, without prior permission of the author.

**title**

PROEFSCHRIFT

ter verkrijging van de graad van doctor aan de  
Technische Universiteit Eindhoven, op gezag van de  
rector magnificus prof.dr.ir. F.P.T. Baaijens, voor een  
commissie aangewezen door het College voor  
Promoties, in het openbaar te verdedigen

door

Carmela Filosa

geboren te Torre del greco, Italië

Dit proefschrift is goedgekeurd door de promotoren en de samenstelling van de promotiecommissie is als volgt:

voorzitter:     prof.dr.  
1<sup>e</sup> promotor:    prof.dr. W.L. IJzerman  
copromotor:     dr. J.H.M. ten Thije Boonkkamp  
leden:

Het onderzoek of ontwerp dat in dit proefschrift wordt beschreven is uitgevoerd in overeenstemming met de TU/e Gedragscode Wetenschapsbeoefening.

# Contents

<b>1</b>	<b>Introduction</b>	<b>3</b>
1.1	Motivation . . . . .	3
1.2	Methods and results . . . . .	3
1.3	Content of this thesis . . . . .	3
<b>2</b>	<b>Illumination optics</b>	<b>5</b>
2.1	Radiometric and photometric variables . . . . .	5
2.2	Reflection and refraction law . . . . .	10
2.3	Fresnel's equations . . . . .	11
<b>3</b>	<b>Ray tracing</b>	<b>19</b>
3.1	Ray tracing for two-dimensional optical systems . . . . .	19
3.2	Monte Carlo ray tracing . . . . .	21
3.3	Quasi-Monte Carlo ray tracing . . . . .	26
<b>4</b>	<b>Ray tracing on phase space</b>	<b>31</b>
4.1	Phase space concept . . . . .	31
4.2	Phase space ray tracing . . . . .	32
4.3	Comparison between MC, QMC and PS ray tracing . . . . .	34
<b>5</b>	<b>Two different approaches to compute the boundaries in target phase space</b>	<b>35</b>
5.1	The $\alpha$ -shapes approach . . . . .	35
5.2	The two-faceted cup . . . . .	35
5.3	Results for a TIR collimator . . . . .	35
5.4	The triangulation refinement approach . . . . .	35
5.5	The two-faceted cup . . . . .	35
5.6	Results for a TIR collimator . . . . .	35
5.7	Results for a Parabolic reflector . . . . .	35
5.8	Results for the Compound Parabolic Concentrator (CPC) . . . . .	35
<b>6</b>	<b>The inverse ray mapping method: analytic approach</b>	<b>37</b>
6.1	Explanation of the method . . . . .	37
6.2	The two-faceted cup . . . . .	37

6.3	Results for the two-faceted cup . . . . .	37
6.4	Results for the multi-faceted cup . . . . .	37
6.5	Discussions . . . . .	37
<b>7</b>	<b>The extended ray mapping method</b>	<b>39</b>
7.1	Explanation of the method . . . . .	39
7.2	Bisection procedure . . . . .	39
7.3	Results for a parabolic reflector . . . . .	39
7.4	Results for two different kind of TIR-collimators . . . . .	39
<b>8</b>	<b>Extended ray mapping method to systems with Fresnel reflection</b>	<b>41</b>
<b>9</b>	<b>Discussion and conclusions</b>	<b>43</b>
<b>A</b>	<b>Implementation of Sobol' sequences</b>	<b>45</b>
A.1	Van der Corput sequences . . . . .	45
A.2	Sobol' sequences . . . . .	46
	<b>Curriculum Vitae</b>	<b>51</b>
	<b>Acknowledgments</b>	<b>53</b>
	<b>Bibliography</b>	<b>55</b>

# List of symbols

$\tau$	time
$Q$	Total energy emitted from a light source or received by a target
$\Phi_r$	Radiant flux
$\Phi$	Luminous flux
$\lambda$	Wavelength
$\Psi_r$	Power per wavelength
$\bar{y}(\lambda)$	Luminosity function
$E$	Illuminance
$d\Omega$	Solid angle
$I$	Intensity
$L$	Luminance
$U$	étendue
$\nu$	Surface normal
$n$	Index of refraction of the medium in which a surface is immersed
$\theta$	Angle between the direction of the solid angle and the normal $\nu$
$n_i$	Index of refraction of the medium in which the incident ray travels
$n_r = n_i$	Index of refraction of the medium in which the reflected ray is located
$n_t$	Index of refraction of the medium in which the transmitted ray travels
$n_{i,t}$	$\frac{n_i}{n_t}$
$\theta_i$	Angle between the incident ray and the normal $\nu$
$\theta_r$	Angle between the reflected ray and the normal $\nu$
$\theta_t$	Angle between the transmitted ray and the normal $\nu$
$\theta_c$	Critical angle
$t_i$	Direction of the incident ray
$t_r$	Direction of the reflected ray
$t_t$	Direction of the transmitted ray
$\nu_j$	Normal to the line $j$
$t_j$	Angle that the ray located on line $j$ forms with respect to the optical axis
$\theta_j$	Angle between the ray and the normal $\nu_j$ to line $j$
$n_j$	Index of refraction of the medium in which line $j$ is located

---



# Chapter 1

## Introduction

1.1 Motivation

1.2 Methods and results

1.3 Content of this thesis



## Chapter 2

# Illumination optics

This chapter provides some concepts of illumination optics used in this thesis. We start explaining the difference between radiometry and photometry. In particular, we focus on the photometric variables, defining them both in three and two dimensions. The reflection and refraction laws and the phenomenon of total internal reflection are explained. The last paragraph of the chapter gives a brief introduction to Fresnel reflection.

### 2.1 Radiometric and photometric variables

Radiometry is concerned with the measurement of electromagnetic radiation across the entire electromagnetic spectrum. Photometry is the subfield of radiometry that takes into account only the portion of the electromagnetic spectrum corresponding to the visible light, [1]. Radiometry deals with radiometric quantities. An important radiometric quantity is the radiant flux  $\Phi_r$  (unit watt, [W]) which is the total energy emitted from a source or received by a target per unit time:

$$\Phi_r = \frac{dQ}{dT}, \quad (2.1.1)$$

where  $Q$  is the energy and  $T$  the time.

In illumination optics the measurement of light is given in terms of the impression that it gives on the human eye. Therefore, illumination optics deals with photometric variables. The most important photometric variables are defined as follows using the same notation adopted by Chaves in [2]. The luminous flux  $\Phi$  (unit lumen, [lm]) is defined as the perceived power of light by the human eye. The radiant and the luminous flux are related by the luminous efficacy function, unit [lm/W], which tells us how many lumen there are for each Watt of power at a given wavelength. The luminous efficacy reaches its maximum at a wavelength of 555 nm where it is equal to 683 lm/W. We may normalize the luminous efficacy function with its maximum value of 683. This normalized function is the dimensionless luminosity function  $\bar{y}(\lambda)$  shown in Figure 2.1 where  $\lambda$  is the wavelength.

The luminous flux corresponding to one Watt of radiation power at any wavelength is given by the product of 683 lm/W and the luminosity function at the same wavelength,

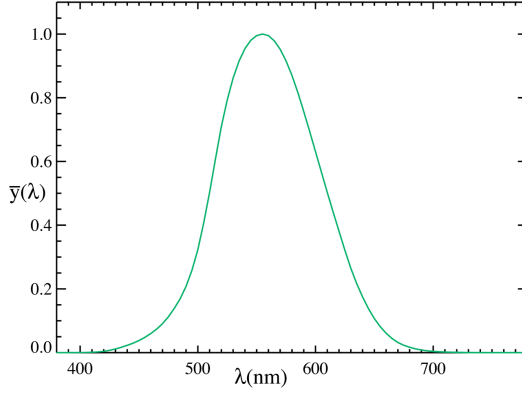


Figure 2.1: Luminosity function  $\bar{y}(\lambda)$ : relation between the eye's sensitivity and the wavelength of light. The luminosity function is dimensionless, [3].

i.e.  $683 \bar{y}(\lambda)$ . Hence, the total luminous flux  $\Phi$  has unit lumen [lm] and it is defined as:

$$\Phi = 683 \int_0^\infty \Psi_r(\lambda) \bar{y}(\lambda) d\lambda \quad (2.1.2)$$

where  $\Psi_r(\lambda)$  is the power in watt per unit wavelength (unit [W/m]).

A beam of light can be described as a collection of parallel light rays, where a light ray can be interpreted as a path along which the energy travels. The luminous flux  $d\Phi$  incident on a surface is called illuminance  $E$  (unit [lm/m<sup>2</sup>]) and is defined as:

$$E = \frac{d\Phi}{dA}, \quad (2.1.3)$$

where  $dA$  is an infinitesimal area receiving radiation. The density of light emitted by a point source in a given direction is determined by the solid angle. The solid angle on a given direction is defined by the infinitesimal surface area  $dS$  of a sphere subtended by the radius of that sphere and by the rays emitted by the center on that direction, [4]. Indicating with  $r$  the radius of the sphere, the infinitesimal solid angle  $d\Omega$  defined by  $dS$  is given by:

$$d\Omega = \frac{dS}{r^2}. \quad (2.1.4)$$

The solid angle on the entire sphere is  $\Omega = 4\pi$ , its unit is the steradian [sr] and it is usually defined on a unit sphere. The luminous intensity  $I$  (unit candela (cd), [cd = lm/sr]) is defined as the luminous flux  $d\Phi$  per solid angle  $d\Omega$  and is given by:

$$I = \frac{d\Phi}{d\Omega}. \quad (2.1.5)$$

The luminance  $L$  (unit [cd/m<sup>2</sup>]) is the luminous flux per unit solid angle  $d\Omega$  and per unit projected area  $\cos\theta dA$  where  $\theta$  is the angle that the normal  $\nu$  to the area  $dA$  makes with the direction of the solid angle  $d\Omega$ , as shown in Figure 2.2.  $L$  is given by:

$$L = \frac{d\Phi}{\cos\theta dA d\Omega}. \quad (2.1.6)$$

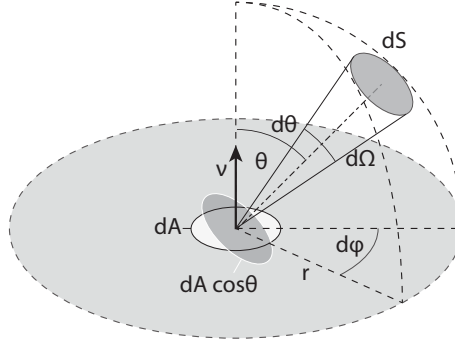


Figure 2.2: Solid angle  $d\Omega$  in a direction making an angle  $\theta$  with the normal to the area  $dA$ .

Note that from (2.1.5) and (2.1.6) we can derive a relation between the intensity and the luminance. The intensity  $I$  emitted by the infinitesimal area  $dA$  is given by:

$$I = \frac{d\Phi}{d\Omega} = L(\mathbf{x}, \theta) \cos \theta dA. \quad (2.1.7)$$

When the luminance is uniform over a finite area  $A$ , the luminous intensity emitted in the direction  $\theta$  is equal to:

$$I(\theta) = L(\theta) A \cos \theta. \quad (2.1.8)$$

Thus, when  $L(\mathbf{x}, \theta)$  does not depend on the position and the direction (i.e.  $L(\mathbf{x}, \theta) = L$ ), we obtain Lambert's cosine law:

$$I(\theta) = I_0 \cos \theta. \quad (2.1.9)$$

where  $I_0 = I(0) = LA$ .

Finally, the étendue  $U$  (unit [m sr]) describes the ability of a source to emit light or the capability of an optical system to receive light, [5]. The quantity  $dU$  is defined as:

$$dU = n^2 \cos \theta dA d\Omega. \quad (2.1.10)$$

where  $n$  is the index of refraction of the medium in which the surface  $A$  is immersed. In optics the étendue is considered to be a volume in phase space (or an area for two-dimensional systems). This concept will be clarified in Chapter 4 in which we treat the phase space in more detail. An important property of the étendue is that it is conserved within an optical system in absence of absorption. We now show, using the approach of Chaves in [2], how conservation of this quantity can be derived. Consider a light ray emitted from an infinitesimal area  $dA_1$  to the area  $dA_2$ . Suppose that the centers of  $dA_1$  and  $dA_2$  are located at a distance  $d$  to each other, see Figure 2.3. Indicating with  $\boldsymbol{\nu}_1$  and  $\boldsymbol{\nu}_2$  the normals to the surfaces  $dA_1$  and  $dA_2$ , respectively and with  $\theta_1$  and  $\theta_2$  the angles that the central ray forms with  $\boldsymbol{\nu}_1$  and  $\boldsymbol{\nu}_2$ , respectively, the flux  $d\Phi_1$  passing through  $dA_2$  coming from  $dA_1$  and the corresponding solid angle

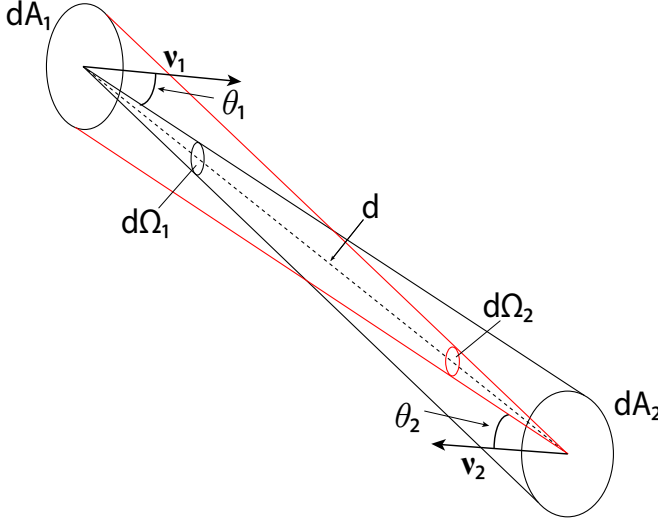


Figure 2.3:  $dA_1$  and  $dA_2$  are two surfaces with normals  $\nu_1$  and  $\nu_2$ , respectively. Their centers are located at a distance  $d$ .  $\theta_1$  and  $\theta_2$  are the angles made by the central ray with the normals  $\nu_1$  and  $\nu_2$ , respectively.

$d\Omega_1$  are defined as:

$$\begin{aligned} d\Phi_1 &= L \cos \theta_1 dA_1 d\Omega_1, \\ d\Omega_1 &= \frac{dA_2 \cos(\theta_2)}{d^2}. \end{aligned} \quad (2.1.11)$$

Similarly, the flux  $d\Phi_2$  passing through  $dA_1$  coming from  $dA_2$  is equal to:

$$\begin{aligned} d\Phi_2 &= L \cos \theta_2 dA_2 d\Omega_2 \\ d\Omega_2 &= \frac{dA_1 \cos \theta_1}{d^2}. \end{aligned} \quad (2.1.12)$$

Then from Eq. (2.1.10) we obtain the following relations:

$$\begin{aligned} dU_1 &= n^2 dA_1 \cos \theta_1 d\Omega_1 = \frac{n^2 dA_1 \cos \theta_1 dA_2 \cos \theta_2}{d^2}, \\ dU_2 &= n^2 dA_2 \cos \theta_2 d\Omega_2 = \frac{n^2 dA_2 \cos \theta_2 dA_1 \cos \theta_1}{d^2} \end{aligned} \quad (2.1.13)$$

for  $dA_1$  and  $dA_2$ , respectively. From the previous equations we can conclude that  $dU_1 = dU_2$  and therefore the étendue  $dU$  is conserved along a beam of light. Since also the flux through the areas  $dA_1$  and  $dA_2$  is conserved, the following relation holds:

$$L := n^2 \frac{d\Phi}{dU} = \text{constant}. \quad (2.1.14)$$

In the optical systems we will consider in this work, the source and the target are located in the same medium (air) with  $n = 1$ , so the luminance  $L$  equals the basic

luminance  $L^* = L/n^2$  at the source and the target of the system.

In this thesis we consider two-dimensional optical systems. Hence, the definitions of the photometric parameters have to be given in two dimensions. An infinitesimal line segment of length  $da$  that emits a light beam and the ray that makes an angle  $\theta$  with the normal  $\nu$  are considered, see Fig. 2.4.

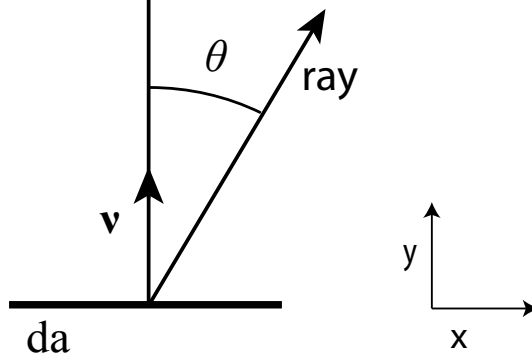


Figure 2.4: Ray emitted by an infinitesimal line segment  $da$  that makes an angle  $\theta$  with respect to the line normal  $\nu$ .

The two-dimensional illuminance (unit  $[\text{lm}/\text{m}]$ ) denotes the luminous flux falling on an infinitesimal line segment of length  $da$  and it is given by:

$$E = \frac{d\Phi}{da} . \quad (2.1.15)$$

The luminous intensity (unit  $[\text{lm}/\text{rad}]$ ) is the luminous flux per angle  $d\theta$ :

$$I = \frac{d\Phi}{d\theta} . \quad (2.1.16)$$

The two-dimensional luminance (unit  $[\text{lm}/(\text{rad} \cdot \text{m})]$ ) is given by:

$$L = \frac{d\Phi}{\cos \theta da d\theta} . \quad (2.1.17)$$

Thus the following relation holds:

$$I = L(x, \theta) \cos \theta da \quad (2.1.18)$$

where  $x$  is a certain position at the light source  $da$ . Finally, the étendue  $dU$  (unit  $[\text{m} \cdot \text{rad}]$ ) in two dimensions is given by:

$$dU = n \cos \theta da d\theta . \quad (2.1.19)$$

In order to determine the light distribution on a surface and to compute the photometric variables on that surface, we need to understand how the light emitted from the source propagates. In the field of geometric optics the light propagation is described by light rays. The propagation of a light ray traveling through different media is determined by the reflection and refraction law. In the following we introduce these two laws and we explain the total internal reflection phenomenon.

## 2.2 Reflection and refraction law

A light ray is described by a position vector  $\mathbf{x}$  on a surface and a direction vector  $\mathbf{t}$  and can be parameterized by the arc length  $s$ . Light rays travel in a homogeneous medium along straight lines, once they hit a reflective surface their direction changes. Denoting with  $\mathbf{t}_i$  the direction of the incident ray and with  $\boldsymbol{\nu}$  the unit normal to the surface at the location of incidence, the direction  $\mathbf{t}_r$  of the reflected ray is given by:

$$\mathbf{t}_r = \mathbf{t}_i - 2(\mathbf{t}_i \cdot \boldsymbol{\nu})\boldsymbol{\nu}, \quad (2.2.1)$$

where the vectors  $\mathbf{t}_i$  and  $\boldsymbol{\nu}$  are unit vectors and  $\mathbf{t}_i \cdot \boldsymbol{\nu}$  indicates the scalar product between  $\mathbf{t}_i$  and  $\boldsymbol{\nu}$ . From Eq. (2.2.1) it follows that the vector  $\mathbf{t}_r$  is a unit vector too, indeed considering the scalar product  $(\mathbf{t}_r, \mathbf{t}_r)$  we conclude:

$$\mathbf{t}_r \cdot \mathbf{t}_r = \mathbf{t}_i \cdot \mathbf{t}_i - 4(\mathbf{t}_i \cdot \boldsymbol{\nu})(\mathbf{t}_i \cdot \boldsymbol{\nu}) + 4(\mathbf{t}_i \cdot \boldsymbol{\nu})^2(\boldsymbol{\nu} \cdot \boldsymbol{\nu}) = 1. \quad (2.2.2)$$

The vectors  $\mathbf{t}_i$ ,  $\mathbf{t}_r$  and  $\boldsymbol{\nu}$  live all in the same plane. Defining the incident angle  $\theta_i$  and the reflective angle  $\theta_r$  such that  $\theta_i, \theta_r \in [0, \pi/2)$ . the reflection law states that  $\theta_i = \theta_r$ , see Fig. 2.5.

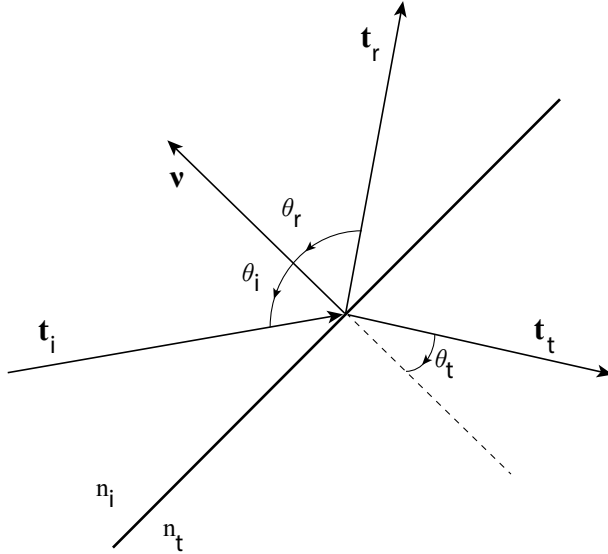


Figure 2.5: Propagation of a ray through two different media with index of refraction  $n_i$  and  $n_t$ .

When a ray propagates through two different media, its direction changes according to the law of refraction. Indicating with  $n_i$  the index of refraction of the medium in which the incident ray travels and with  $n_t$  the index of refraction of the medium of the transmitted ray, the direction  $\mathbf{t}_t$  of the transmitted ray is given by:

$$\mathbf{t}_t = n_{i,t} \mathbf{t}_i + \left[ \sqrt{1 - n_{i,t}^2 + n_{i,t}^2 (\boldsymbol{\nu} \cdot \mathbf{t}_i)^2} - n_{i,t} (\boldsymbol{\nu} \cdot \mathbf{t}_i) \right] \boldsymbol{\nu}, \quad (2.2.3)$$



where  $n_{i,t} = n_i/n_t$ , [2]. Note that in Eq. (2.2.1) the direction of the normal  $\boldsymbol{\nu}$  to the surface is not relevant for the computation of the direction of the reflective ray, since:

$$\mathbf{t}_r = \mathbf{t}_i - 2(\mathbf{t}_i \cdot \boldsymbol{\nu})\boldsymbol{\nu} = \mathbf{t}_i - 2(\mathbf{t}_i \cdot -\boldsymbol{\nu})(-\boldsymbol{\nu}), \quad (2.2.4)$$

however, this is not the case for Eq. (2.2.3), therefore in the latter case we need to specify the direction of  $\boldsymbol{\nu}$  which is usually chosen in such a way that the angle that it forms with the incident ray  $\mathbf{t}_i$  is smaller than or equal to  $\pi/2$ . Hence, if  $(\mathbf{t}_i, \boldsymbol{\nu}) \leq 0$  the normal  $\boldsymbol{\nu}$  directed inside the same medium in which travels the incident ray is taken as in Fig. 2.5, otherwise the normal  $-\boldsymbol{\nu}$  directed inside the same medium in which the transmitted ray will travel has to be considered.

Eq. (2.2.3) is only valid for

$$1 - n_{i,t}^2 + n_{i,t}^2(\boldsymbol{\nu} \cdot \mathbf{t}_i)^2 \geq 0 \quad (2.2.5)$$

which implies that

$$\frac{n_t}{n_i} \geq \sqrt{1 - (\boldsymbol{\nu} \cdot \mathbf{t}_i)^2} \quad (2.2.6)$$

from which we obtain:

$$n_t \geq n_i \sin \theta_i. \quad (2.2.7)$$

The angle  $\theta_c$  for which the equality holds is

$$\theta_c = \arcsin\left(\frac{n_t}{n_i}\right) \quad (2.2.8)$$

and it is called the critical angle, [2]. When the incident angle  $\theta_i$  is exactly equal to the critical angle  $\theta_c$ , the square root in Eq. (2.2.3) is zero and the inner product  $(\mathbf{t}_t, \boldsymbol{\nu}) = 0$ , hence the transmitted ray propagates parallel to the refractive surface. When  $\theta_i > \theta_c$  the light ray is no longer refracted but is only reflected by the surface. This phenomenon is called total internal reflection (TIR). When TIR occurs, 100% of light is reflected and there is no loss of energy. Therefore, optical systems designed such that rays are reflected by TIR are very efficient. Light that hits an ordinary refractive surface can be reflected and refracted. The energy that is reflected and refracted is determined by the Fresnel's coefficients. In the next paragraph an overview of the Fresnel coefficients is given.

## 2.3 Fresnel's equations

In order to derive Fresnel's equations we need to describe light as an electromagnetic wave. It is therefore useful to study the light propagation from the perspective of electromagnetic theory which gives information about the incident, reflected and transmitted radiant flux density that are denoted with  $E_i$ ,  $E_r$  and  $E_t$ , respectively. Any component of the electric field  $\mathcal{E}$  can be written as

$$\mathcal{E}(\mathbf{x}, \tau) = \mathcal{E}_0(\mathbf{x})e^{i(\mathbf{k} \cdot \mathbf{x} - \omega \tau)} \quad (2.3.1)$$

where  $\mathbf{x}$  is the position vector and  $T$  is the time. The amplitude  $\mathcal{E}_0(\mathbf{x})$  is constant in time and  $\omega = \frac{ck}{n}$  is the value of the angular frequency with  $c$  the velocity of light

and  $n$  the index of refraction in which the wave is traveling, which is the ratio of the speed of light  $c$  in vacuum and the speed of light  $v$  in the material. Note that the angular frequency can be also written as  $\omega = vk$ , in particular when a wave travels in vacuum  $n = 1$  and  $\omega = ck$ . The vector  $\mathbf{k}$  has the same direction of the wave and its absolute value  $|\mathbf{k}| = k = \frac{2\pi}{\lambda}$  is the wave number in vacuum, with  $\lambda$  the wavelength. Similarly, the magnetic field has the form:

$$\mathcal{B}(\mathbf{x}, \tau) = \mathcal{B}_0(\mathbf{x})e^{i(\mathbf{k} \cdot \mathbf{x} - \omega\tau)}. \quad (2.3.2)$$

Light can be seen as an electromagnetic wave, that is an oscillating electric field  $\mathcal{E}$  and an oscillating magnetic field  $\mathcal{B}$  which propagates always perpendicular to  $\mathcal{E}$ . The electric field oscillates perpendicular to the wave propagation. Light is said to be polarized if the direction of the electric field is well defined. When the electric field propagates in different directions we talk about unpolarized light. By convention, we refer to the light's polarization as the direction of the electric field  $\mathcal{E}$ , [6] with respect to the incident plane that is defined by the incident and reflected rays as is shown in Fig. 2.6.

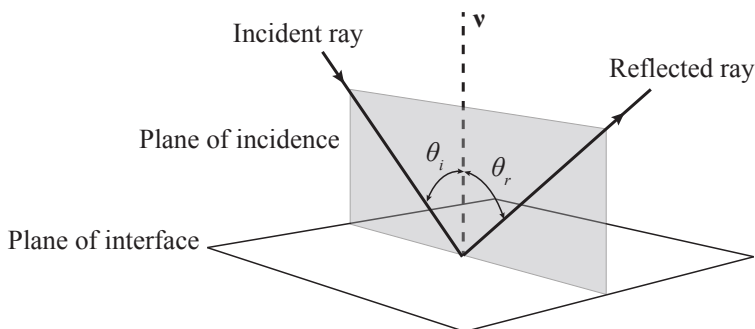


Figure 2.6: Light ray that hits a mirror located on the reflecting plane. The incident and the reflected ray leave in the same plane of the normal to the mirror that is called plane of incident.

In order to derive the Fresnel's coefficients the polarization of light must to be taken into account. Those coefficients are obtained considering Maxwell's equations and the boundary conditions due to the conservation of energy. The details of Fresnel's equations are widely explained in the literature. In the following we provide Fresnel coefficients and we briefly explain their physical interpretation. We refer the reader to [7, 8] for more details. Fresnel's coefficients can also be derived using a different approach that does not involve Maxwell's equations, this method is explained in [9]. The following particular cases of light's polarization need are considered.

1.  $\mathcal{E}$  is perpendicular to the plane of incidence (see Fig. 2.7). In this case light is said to be *s*-polarized.
2.  $\mathcal{E}$  is parallel to the plane of incidence (see Fig. 2.8). In this case light is said to be *p*-polarized.

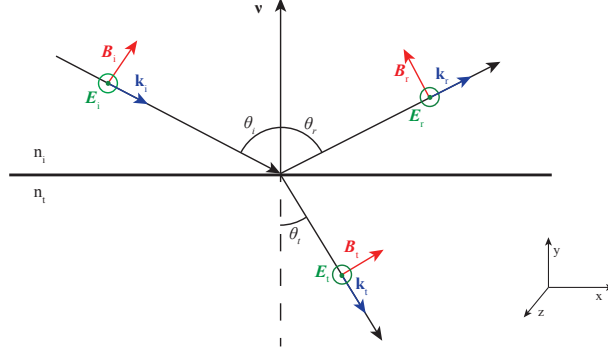


Figure 2.7: Propagation of an electromagnetic wave where  $\mathcal{E}$  is perpendicular to the incident plane. The components of  $\mathcal{E}$  are indicated with the green circles. The components of  $\mathcal{B}$  are indicated with red arrows.

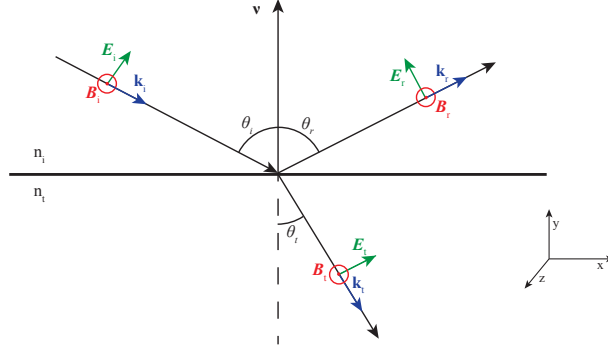


Figure 2.8: Propagation of an electromagnetic wave where  $\mathcal{E}$  is parallel to the incident plane. The components of  $\mathcal{B}$  are indicated with the red circle. The components of  $\mathcal{E}$  are indicated with green arrows.

Energy conservation gives the boundary conditions of the electromagnetic field at the plane of the interface (which is perpendicular to the incident plane). In the following we derive Fresnel's coefficients for case 1. Similarly, the Fresnel's coefficients can be derived for the second case.

For  $s$ -polarized light the tangential components of  $\mathcal{E}$  and  $\mathcal{B}/\mu$  across the boundary between the two different media must be continuous. The continuity of the tangential component of  $\mathcal{E}$  leads to:

$$|\mathcal{E}_{0i}| + |\mathcal{E}_{0r}| = |\mathcal{E}_{0t}|, \quad (2.3.3)$$

while the continuity of the tangential component of  $\mathcal{B}/\mu$  gives:

$$-\frac{|\mathcal{B}_{0i}|}{\mu_i} \cos \theta_i + \frac{|\mathcal{B}_{0r}|}{\mu_r} \cos \theta_r = -\frac{|\mathcal{B}_{0t}|}{\mu_t} \cos \theta_t, \quad (2.3.4)$$

where the negative sign in front of  $|\mathcal{B}_{0,i}|$  and  $|\mathcal{B}_{0,t}|$  is due to the convention that a positive direction is considered with increasing  $x$ . Since  $\mathcal{B} = \mathcal{E}/v$ , Eq. (2.3.4) can be written as

$$\frac{1}{\mu_i v_i} (|\mathcal{E}_{0,i}| - |\mathcal{E}_{0,r}|) \cos \theta_i = \frac{1}{\mu_t v_t} |\mathcal{E}_{0,t}| \cos \theta_t, \quad (2.3.5)$$

where we employed the fact that  $v_i = v_r$ , and  $\theta_i = \theta_r$ . Using Eq. (2.3.1) and  $n = c/v$ , the previous equation becomes:

$$\frac{n_i}{\mu_i} (|\mathcal{E}_{0,i}| - |\mathcal{E}_{0,r}|) \cos \theta_i = \frac{n_t}{\mu_i} |\mathcal{E}_{0,t}| \cos \theta_t \quad (2.3.6)$$

Finally, assuming that  $\mu_i = \mu_t = \mu_0$  and employing Eq. (2.3.3) we obtain:

$$\begin{aligned} r_s &= \frac{|\mathcal{E}_{0,r}|_s}{|\mathcal{E}_{0,i}|_s} = \frac{n_i \cos \theta_i - n_t \cos \theta_t}{n_i \cos \theta_i + n_t \cos \theta_t}, \\ t_s &= \frac{|\mathcal{E}_{0,t}|_s}{|\mathcal{E}_{0,i}|_s} = \frac{2n_i \cos \theta_i}{n_i \cos \theta_i + n_t \cos \theta_t}. \end{aligned} \quad (2.3.7)$$

The coefficients  $r_s$  and  $t_s$  are amplitude coefficients for the reflected and transmitted light. They are the perpendicular components of  $r$  and  $t$  for  $s$ -polarized light. Using Snell's law, that is  $n_i \sin \theta_i = n_t \sin \theta_t$ , the relations for  $r_s$  and  $t_s$  are simplified as follows:

$$\begin{aligned} r_s &= -\frac{\sin(\theta_i - \theta_t)}{\sin(\theta_i + \theta_t)}, \\ t_s &= -\frac{2 \sin \theta_t \cos \theta_i}{\sin(\theta_i + \theta_t)}. \end{aligned} \quad (2.3.8)$$

A similar argument for the  $p$ -polarized light leads to the calculation of the parallel components  $r_p$  and  $t_p$  of  $r$  and  $t$ . In case  $\mathcal{E}$  is parallel to the plane of incidence the amplitude coefficients are:

$$\begin{aligned} r_p &= \frac{n_t \cos \theta_i - n_i \cos \theta_t}{n_i \cos \theta_t + n_t \cos \theta_i}, \\ t_p &= \frac{2n_i \cos \theta_i}{n_i \cos \theta_t + n_t \cos \theta_i}, \end{aligned} \quad (2.3.9)$$

and their simplified relations are:

$$\begin{aligned} r_p &= \frac{\tan(\theta_i - \theta_t)}{\theta_i + \theta_t}, \\ t_p &= \frac{2 \sin \theta_t \cos \theta_i}{\sin(\theta_i + \theta_t) \cos(\theta_i - \theta_t)}. \end{aligned} \quad (2.3.10)$$

Furthermore, it can be checked that

$$\begin{aligned} t_s - r_s &= 1, \\ t_p + r_p &= 1. \end{aligned} \quad (2.3.11)$$

The amplitude coefficients are shown in Fig. 2.9 for the case in which light travels from a less dense to a more dense medium ( $n_i < n_t$ ), that is external reflection. In

Fig. 2.10 the reflection coefficients are shown for the case in which  $n_i > n_t$ , that is internal reflection. Note from Fig. 2.9 that  $r_p$  approaches 0 when  $\theta_i$  approaches to  $\theta_p$  and it gradually decreases reaching  $-1$  for an incident angle  $\theta_i = 90^\circ$ . The angle  $\theta_p$  is called Brewster's angle or polarization angle as only the component perpendicular to the incident plane is reflected at that angle and therefore light is perfectly polarized. Similarly, Fig. 2.10 shows that  $r_p = 0$  for  $\theta_i = \theta_{p'}$ . It can be show that  $\theta_p + \theta_{p'} = 90^\circ$ . Both  $r_p$  and  $r_s$  reach 1 when  $\theta_i = \theta_c$ .  $\theta_c$  is called the critical angle. Light that hits the incident plane with an incident angle equal to or greater than the critical angle is totally reflected back and no transmitted light is observed. This phenomenon is called total internal reflection.

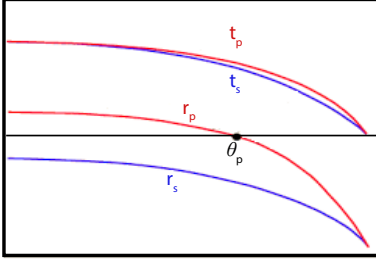


Figure 2.9: Amplitude coefficients of reflection and transmission as a function of the incident angle  $\theta_i$  in the case of external reflection, i.e.  $n_t < n_i$  ( $n_t = 1$  and  $n_i = 1.5$ ).  $\theta_p$  is the polarization angle, [8].

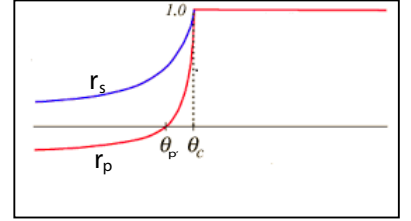


Figure 2.10: Reflection coefficients as a function of the incident angle  $\theta_i$  in the case of internal reflection, i.e.  $n_t > n_i$  ( $n_t = 1.5$  and  $n_i = 1$ ).  $\theta_{p'}$  is the polarization angle and  $\theta_c$  is the critical angle, [8].

The we introduce the Poynting vector  $\mathbf{P}$  that defines the energy flux of an electromagnetic field. It is measured in  $[\text{W}/\text{m}^2]$ , and it is given by:

$$\mathbf{P} = \frac{1}{\mu} (\mathbf{\mathcal{E}} \times \mathbf{\mathcal{B}}), \quad (2.3.12)$$

where  $\mu = \frac{1}{\epsilon v^2}$  is the permeability and  $\epsilon$  the permittivity of the medium. In the following, the parameters for vacuum are indicated with the subscript 0. All quantities defined in the media of the incident, reflective and transmitted light are indicated with the subscripts i, r and t, respectively. Optical rays are perpendicular to the wave front of an electromagnetic wave and parallel to the Poynting vector, [10]. The irradiance  $E$  is defined as the average energy that crosses in unit time a unit area  $A$  perpendicular to the direction of the energy flow. Therefore, defining the average of the vector  $\mathbf{P}$  over the time as:

$$\langle \mathbf{P} \rangle_T = \frac{1}{T} \int_0^T \mathbf{P} dt \quad (2.3.13)$$

we can write the irradiance  $E$  as:

$$E = \langle \mathbf{P} \rangle_\tau = v\epsilon |\mathbf{\mathcal{E}}|^2. \quad (2.3.14)$$

Considering a beam of light that hits a surface such that an area  $A$  is illuminated, the incident, reflected and transmitted beams are  $\mathbf{E}_i A \cos \theta_i$ ,  $\mathbf{E}_r A \cos \theta_r$  and  $\mathbf{E}_t A \cos \theta_t$ ,

respectively. The reflectance  $\mathcal{R}$  is the ratio of the reflected power to the incident power:

$$\mathcal{R} = \frac{|\mathbf{E}_r| \cos \theta_r}{|\mathbf{E}_i| \cos \theta_i} = \frac{|\mathcal{E}_{0r}|^2}{|\mathcal{E}_{0i}|^2} = r^2 \quad (2.3.15)$$

where the second equality holds because  $v_i = v_t$ ,  $\varepsilon_i = \varepsilon_t$  and  $\theta_i = \theta_t$ . Similarly, the transmittance  $\mathcal{T}$  is the ratio between the transmitted to the incident power:

$$\mathcal{T} = \frac{|\mathbf{E}_t| \cos \theta_t}{|\mathbf{E}_r| \cos \theta_r} = \frac{n_t \cos \theta_t}{n_t \cos \theta_i} \frac{|\mathcal{E}_{0t}|^2}{|\mathcal{E}_{0i}|^2} = \frac{n_t \cos \theta_t}{n_t \cos \theta_i} t^2. \quad (2.3.16)$$

Employing total energy conservation, that is:

$$\mathbf{E}_i A \cos \theta_i = \mathbf{E}_r A \cos \theta_r + \mathbf{E}_t A \cos \theta_t, \quad (2.3.17)$$

we can easily prove that:

$$\mathcal{R} + \mathcal{T} = 1. \quad (2.3.18)$$

The parallel and perpendicular components of  $\mathcal{R}$  and  $\mathcal{T}$  are:

$$\begin{aligned} \mathcal{R}_p &= r_p^2, \\ \mathcal{T}_p &= \frac{n_t \cos \theta_t}{n_t \cos \theta_i} t_p^2, \\ \mathcal{R}_s &= r_s^2, \\ \mathcal{T}_s &= \frac{n_t \cos \theta_t}{n_t \cos \theta_i} t_s^2. \end{aligned} \quad (2.3.19)$$

it can be show that

$$\begin{aligned} \mathcal{R}_s + \mathcal{R}_p &= 1, \\ \mathcal{T}_s + \mathcal{T}_p &= 1. \end{aligned} \quad (2.3.20)$$

For normal incidence, i.e.  $\theta_i = 0$ , there is no polarization and Eqs. (2.3.19) lead to:

$$\begin{aligned} \mathcal{R} = \mathcal{R}_p = \mathcal{R}_s &= \left( \frac{n_i - n_t}{n_t + n_i} \right)^2, \\ \mathcal{T} = \mathcal{T}_p = \mathcal{T}_s &= \frac{4n_i n_t}{(n_t + n_i)^2}. \end{aligned} \quad (2.3.21)$$

Many common light sources such as sunlight, halogen lighting, LED spotlights, and incandescent bulbs produce unpolarized light. In case of unpolarized light the amount of reflected and transmitted light is given by the average of reflectance  $\mathcal{R}$  and transmittance  $\mathcal{T}$  calculated considering first  $p$ -polarized light and then  $s$ -polarization, that is:

$$\begin{aligned} \mathcal{R} &= \frac{\mathcal{R}_p + \mathcal{R}_s}{2}, \\ \mathcal{T} &= \frac{\mathcal{T}_p + \mathcal{T}_s}{2}, \end{aligned} \quad (2.3.22)$$

where  $\mathcal{R}_p$ ,  $\mathcal{R}_s$ ,  $\mathcal{T}_p$  and  $\mathcal{T}_s$  are given in Eqs. (2.3.19).

With this overview we conclude this chapter. The notions given in Section 2.1 will be used in the entire thesis as our goal is to study the distribution of light at the target of some optical systems. In particular we will focus on the computation of the output intensity distribution. The reflection and refraction laws explained in Section 2.2 are needed to determine how the optical system changes the ray's direction every time that it hits a surfaces (or a line in the two-dimensional case). In Chapters 3, 4, 5, 6 and 7 only systems where the reflection and refraction laws play a role are considered. Systems with Fresnel reflection are treated in the last chapter. The amount of reflected and transmitted light is calculated using the Fresnel's equation (introduced in the last paragraph of this chapter). Since, we restrict ourselves to two-dimensional systems, the value of reflectance and transmittance will be computed using Eqs. (2.3.22).





# Chapter 3

## Ray tracing

Ray tracing is a geometric problem that calculates the transport of light within optical systems. It is a forward method which uses single rays to describe light propagation. Given an optical system and a set of rays at the source, ray tracing relates the emitted light with its output distribution. The influence of diffraction on the transport of a ray is neglected and geometrical modeling of an optical system needs to be considered. Although the method can be implemented for two or more dimensions and for any optical system, here we consider the two-dimensional case only. From now on, we will thus refer to optical lines instead of optical surfaces. The two-dimensional case is particularly relevant because it is a good test case to demonstrate the performance of new methods. Optical designers often start with 2D systems, where only the meridional plane is taken into account because it gives a good prediction of the target distribution of the rays (see [11], chapter 4, p.50 – 65). However, the two-dimensional case has limitations. For example, it may not identify skew rays that are turned back by the system, with the consequence that a 2D analysis cannot guarantee a proper treatment of non meridional rays in 3D. In this chapter we consider systems where only reflection and refraction laws are taken into account.

### 3.1 Ray tracing for two-dimensional optical systems

Ray tracing consists of tracing each ray through the optical system. Every ray emitted from the source is followed until it reaches the target. During its propagation it can encounter optical components which change its direction. It is thus considered to be a broken line which vertices are given by its location coordinates on every optical component encountered. The ray tracing procedure is constructed such that the position and the direction of the rays are calculated on every optical lines that they hit until they reach the target. Given a Cartesian coordinate system  $(x, z)$ , a two-dimensional optical system symmetric with respect to the  $z$ -axis is defined. Hence, usually the optical axis coincides with the  $z$ -axis. The optical system is formed by a source  $S$ , a target  $T$  and some optical components labeled with indexes  $j$  where  $j \in \{2, \dots, Nl - 1\}$  and  $Nl$  indicates the number of lines that form the system.  $S$  and  $T$  are indicated with the indexes 1 and  $Nl$ , respectively. The index of refraction of the medium in which line  $j$  is located is indicated with  $n_j$ . Every ray emitted by  $S$  (line 1)

can hit some optical components  $j \in \{2, \dots, Nl - 1\}$  before reaching  $T$  (line  $Nl$ ). The intersection point of the rays with line  $j$  are  $(x_j, z_j)_{j=1, \dots, Nl}$  and,  $\mathbf{s}_j = (-\sin t_j, \cos t_j)$  indicates the direction vector of the rays that leave  $j$ , with  $t_j$  the angle that the ray forms with respect to the optical axis measured counterclockwise. As we consider only forward rays, the angles  $t_j \in (-\pi/2, \pi/2)$ . Therefore, a ray segment between  $(x_j, z_j)$  and  $(x_k, z_k)$  with  $k \neq j$  is parameterized in real space by:

$$\mathbf{r}(s) = \begin{pmatrix} x_j - s \sin t_j \\ z_j + s \cos t_j \end{pmatrix} \quad 0 < s \leq s_{\max}, \quad (3.1.1)$$

where  $s$  denotes the arc-length and  $s_{\max}$  is the maximum value that it can assume. Fig. 3.1 shows an example where a single ray is traced inside a very simple optical system, the so-called two-faceted cup. The light source  $S = [-a, a]$  (line 1) and the

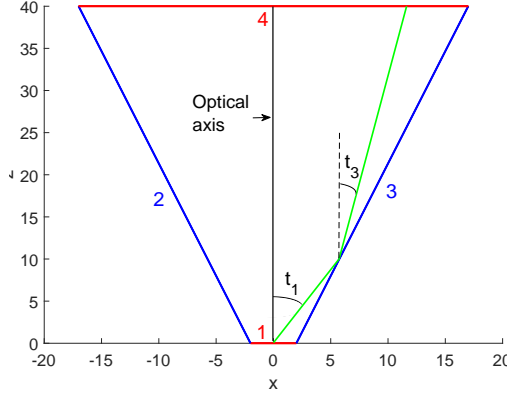


Figure 3.1: Shape of the two-faceted cup. Each line of the system is labeled with a number. The source  $S = [-2, 2]$  (line number 1) is located on the  $x$ -axis. The target  $T = [-17, 17]$  (line 4) is parallel to the source and is located at a height  $z = 40$ . The left and right reflectors (line 2 and 3) connect the source with the target.

target  $T = [-b, b]$  (line 4) are two segments normal to the  $z$ -axis, where  $a = 2$  and  $b = 17$ . The left and right reflectors (line 2 and 3) are oblique segments that connect the source and the target. All the optical lines  $j \in \{1, \dots, 4\}$  are located in air, thus the refractive index is  $n_j = 1$  for every  $j$ .

In order to compute the target photometric variables, we need to know how the optical system influences the direction of the rays when they hit an optical line. Ray tracing relates the position coordinates  $(x_1, z_1)$  and the direction vector  $\mathbf{s}_1$  of every ray at the source  $S$  with the corresponding position  $(x_{Nl}, z_{Nl})$  and direction  $\mathbf{s}_{Nl}$  at the target  $T$ . In the following we will use often the target coordinates of the rays thus, to simplify the notation, we do not write the subscript  $Nl$  for the target coordinates. Hence, from now on, we write  $(x, z)$  instead of  $(x_{Nl}, z_{Nl})$ ,  $t$  instead of  $t_{Nl}$  and  $\mathbf{s}$  instead of  $\mathbf{s}_{Nl}$  for the target coordinates. The ray tracing algorithm can be outlined as follows.

1. Given a ray that leaves  $S$  with initial position  $(x_1, z_1)$  and initial direction  $\mathbf{s}_1 = (-\sin t_1, \cos t_1)$ , use Eq. (3.1.1) to implement the ray parametrization  $\mathbf{r}(s_1)$ ;

2. Compute the coordinates  $(x_k, z_k)_{k=1 \dots, N_l}$  of the intersection point of the parameterized ray  $\mathbf{r}(s_1)$  with all the lines that it hits;
  - a) If the shape of the lines is described by an analytical equation, the intersection points are determined analytically;
  - b) If there is no analytic description for the optical lines, the intersections need to be determined using iterative methods;
3. Determine the closest line  $j$  that the forward ray encounters;
4. If  $j = N_l$  stop the procedure, the target ray's coordinates  $(x, z)$  and  $\mathbf{s}$  are found.
5. Calculate the normal  $\boldsymbol{\nu}_i$  to line  $i$  at the point  $(x_i, z_i)$ ;
6. Compute the new ray direction  $\mathbf{s}_j$  of the ray that leaves line  $j$  at the point  $(x_i, z_i)$ :
  - a) if the incident line is a reflective line,  $\mathbf{s}_j$  is given by Eq. (2.2.1);
  - b) if the incident line is a refractive line,  $\mathbf{s}_j$  is given by Eq. (2.2.3);
7. Restart the procedure from 1. for the ray that leaves line  $j$  instead of  $S$ . Consider as initial ray position coordinates  $(x_i, z_i)$  instead of  $(x_1, z_1)$  and as initial ray direction  $\mathbf{s}_j = (-\sin t_j, \cos t_j)$  instead of  $\mathbf{s}_1$ .

The procedure explained above is repeated for every ray traced through the system, [12]. Once the target position and the direction of every ray traced are computed, the target photometric variables can be calculated using the definitions explained in the previous chapter, see section 2.1.

There are different ways to implement the ray tracing procedure. The efficiency of the ray tracing can be related with the distribution of the rays at the source. If the initial position and direction of the rays are chosen randomly we have Monte Carlo (MC) ray tracing. This is a very common method in non-imaging optics as it is very powerful and easy to implement. MC ray tracing will be explained in details in the next paragraph. If the rays are chosen from a so-called low discrepancy sequence we have the Quasi-Monte Carlo (QMC) ray tracing. This will be discussed in Section 3.3.

## 3.2 Monte Carlo ray tracing

Before explain MC ray tracing we give a general introduction to the MC methods approximate computation of integrals. Given an interval  $D = [\mathbf{a}, \mathbf{b}]$  with  $\mathbf{a} = (a_1, \dots, a_d)$  and  $\mathbf{b} = (b_1, \dots, b_d)$  elements of  $\mathbb{R}^d$  such that  $[\mathbf{a}, \mathbf{b}] = [a_1, b_1] \times \dots \times [a_d, b_d]$ , a function  $f: [\mathbf{a}, \mathbf{b}] \subset \mathbb{R}^d \mapsto \mathbb{R}$  and a random variable  $\mathbf{y} \in D$  with probability density function  $\rho(\mathbf{y})$ , the expected value of  $f$  with respect of  $\rho$  is

$$\mathbb{E}[f] = \int_D f(\mathbf{y})\rho(\mathbf{y})d\mathbf{y}. \quad (3.2.1)$$

If  $\rho$  is a uniform probability density function,

$$\mathbb{E}[f] = \int_D f(\mathbf{y})\rho(\mathbf{y})d\mathbf{y} = \frac{1}{(\mathbf{b} - \mathbf{a})} \int_D f(\mathbf{y})d\mathbf{y}. \quad (3.2.2)$$

Monte Carlo approximates Eq. (3.2.2) by

$$S_N(f) = \frac{1}{N} \sum_{i=1}^N f(\mathbf{y}_i) \quad (3.2.3)$$

$\{\mathbf{y}_i\}_{i=1, \dots, N} \in D$  are independent samples of the density function  $\rho$ , [13]. According to the strong law of large numbers,

$$\Pr\left(\lim_{N \rightarrow \infty} \frac{1}{N} \sum_{i=1}^N f(\mathbf{y}_i) = \mathbb{E}[f(\mathbf{y})]\right) = 1. \quad (3.2.4)$$

Therefore,

$$\mathbb{E}[f] = \int_D f(\mathbf{y}) \rho(\mathbf{y}) d\mathbf{y} \approx \frac{1}{N} \sum_{i=1}^N f(\mathbf{y}_i). \quad (3.2.5)$$

Suppose that  $f$  has variance  $\text{Var}[f] = \sigma^2[f]$ , then

$$\text{Var}[S_N(f)] = \mathbb{E}[(S_N(f) - \mathbb{E}[S_N(f)])^2] = \mathbb{E}[(S_N(f) - \mathbb{E}[f])^2] = \sigma[f]^2/N, \quad (3.2.6)$$

where the second equality follows from the obvious relation

$$\mathbb{E}[S_N(f)] = \frac{1}{N} \sum_{i=1}^N \mathbb{E}[f(\mathbf{y}_i)]. \quad (3.2.7)$$

Let us denote the integration error with:

$$\text{err}(f, S_N) = \int_D f(\mathbf{y}) \rho(\mathbf{y}) d\mathbf{y} - S_N(f), \quad (3.2.8)$$

we obtain that

$$\mathbb{E}[|\text{err}(f, S_N)|] \leq \sqrt{\mathbb{E}[\text{err}(f, S_N)^2]} = \frac{\sigma[f]}{\sqrt{N}}. \quad (3.2.9)$$

Hence, the absolute value of the integration error is, on average, bounded by  $\sigma[f]/\sqrt{N}$ , where  $\sigma[f]$  is the standard deviation of  $f$ , [14]. It is very important to note that  $\text{err}(f, S_N)$  does not depend on the dimension  $d$  of  $f$ .

MC technique can be combined with the ray tracing procedure in order to compute the light distribution at the target of an optical system. In MC ray tracing the position and the direction of every ray at the source are chosen randomly. In the two-dimensional case ( $d=2$ ), for every ray we need to choose one position coordinate  $x_1$  at the source and one angular coordinate  $t_1$  at the target, while the  $z_1$  coordinate of every ray at the source is always given (for instance, for the two-faceted cup in Fig. 3.1,  $z_1 = 0$  for every ray). Therefore, given a set of random variables  $\{\mathbf{y}_1, \dots, \mathbf{y}_N\} \in [\mathbf{a}, \mathbf{b}] \subset \mathbb{R}^2$ , the initial position coordinate  $x_1$  of the  $k$ -th ray corresponds to the first component of the  $k$ -th random variable  $\mathbf{y}_k$  and, the starting angular coordinate  $t_1$  of the  $k$ -th ray corresponds to the second component of the  $k$ -th random variable  $\mathbf{y}_k$ . Next, rays with those random coordinates at  $S$  are traced from  $S$  to  $T$  and, a probabilistic interpretation of the output photometric variables is provided. In particular, we are interested in the total target intensity  $I$  which is computed as a

function of the angular coordinate  $t$ . The MC intensity is calculated dividing the target into intervals of equal length, the so-called bins. A partitioning  $P_1 : -\pi/2 = t_0 < t_1 < \dots < t_{\text{Nb}} = \pi/2$  of the interval  $[-\pi/2, \pi/2]$  is defined where Nb is the number of bins in  $P_1$ . We remark that, with a slight abuse of notation, we indicated the angular coordinates of the rays at the target (line Nl) with  $t_j$  instead of  $t_{\text{Nl},j}$  for every  $j \in \{0, \dots, \text{Nb}\}$ .

The normalized approximated intensity  $I_{\text{MC}}(t)$  is a piecewise constant function, whose value over the  $j$ -th bin is the ratio between the number of rays that fall into that bin  $\text{Nr}[t_{j-1}, t_j]$  and the total number of rays traced  $\text{Nr}[-\pi/2, \pi/2]$ . Hence,  $I_{\text{MC}}$  is defined by

$$I_{\text{MC}}(t) = \frac{\text{Nr}[t_{j-1}, t_j]}{\text{Nr}[-\pi/2, \pi/2]} \quad \text{for } t \in [t_{j-1}, t_j]. \quad (3.2.10)$$

The output intensity is computed from the value of the intensity  $I_{\text{MC}}(t_{j-1/2})$  along the direction  $t_{j-1/2} = (t_{j-1} + t_j)/2$  for every bin  $[t_{j-1}, t_j]_{j=1, \dots, \text{Nb}}$ . The intensity  $I_{\text{MC}}(t_{j-1/2})$  gives an estimate of the probability that a ray reaches the target with an angle in the  $j$ -th interval  $[t_{j-1}, t_j]$  of the partitioning  $P_1$ . This probability  $P_{j,\Delta t}$  is given by

$$P_{j,\Delta t} = \Pr(t_{j-1} \leq t < t_j) = \frac{\int_{t_{j-1}}^{t_j} I(t) dt}{\int_{-\pi/2}^{\pi/2} I(t) dt}, \quad (3.2.11)$$

where  $I(t)$  is the output intensity (not normalized). Note that  $\sum_{j=1}^{\text{Nb}} P_{j,\Delta t} = 1$ . From the mean value theorem for the function  $I(t)$ , continuous in  $[t_{j-1}, t_j]$ , there exists a value  $t_k \in [t_{j-1}, t_j]$  for which the integral at the numerator of the previous equation can be written as

$$\int_{t_{j-1}}^{t_j} I(t) dt = \Delta t I(t_k). \quad (3.2.12)$$

Hence,  $P_{j,\Delta t}$  is proportional to the size  $\Delta t = (t_{\text{Nb}} - t_0)/\text{Nb}$  of the intervals, i.e. inversely proportional to the number of bins Nb of the partitioning  $P_1$ . Indicating with  $\Phi = \int_{-\pi/2}^{\pi/2} I(t) dt$  the total flux (measured in lumen [lm]), the error between the intensity  $I(t_{j-1/2})$  and the averaged MC intensity  $\Phi I_{\text{MC}}(t_{j-1/2})/\Delta t$  is given by

$$\begin{aligned} \left| I(t_{j-1/2}) - \frac{\Phi}{\Delta t} I_{\text{MC}}(t_{j-1/2}) \right| &\leq \\ \left| I(t_{j-1/2}) - \frac{1}{\Delta t} \int_{t_{j-1}}^{t_j} I(t) dt \right| &+ \\ \frac{1}{\Delta t} \left| \int_{t_{j-1}}^{t_j} I(t) dt - \Phi I_{\text{MC}}(t_{j-1/2}) \right|. \end{aligned} \quad (3.2.13)$$

The first term of the right hand side of inequality (3.2.13) gives an estimate of how much the averaged intensity  $\frac{1}{\Delta t} \int_{t_{j-1}}^{t_j} I(t) dt$  differs from the exact intensity  $I(t_{j-1/2})$ . This term is due to the discretization of the target and therefore it depends on the number of bins Nb considered. Substituting  $I(t)$  with its Taylor expansion around the point  $t_{j-1/2}$  we obtain that this term is proportional to the square of the size of the bins. Therefore,

$$\left| I(t_{j-1/2}) - \frac{1}{\Delta t} \int_{t_{j-1}}^{t_j} I(t) dt \right| = C_1/\text{Nb}^2 \quad (3.2.14)$$

with  $C_1 > 0$  a certain constant.

The second part of the right hand side of inequality (3.2.13) gives an estimate of the MC error and therefore it depends also on the number of rays traced. In order to show how this term decreases as a function of the number of rays traced, we define the random variable  $X_j(t)$  as the variable that is equal to 1 if the ray with angular coordinate  $t$  is inside the interval  $[t_{j-1}, t_j]$  and equal to 0 otherwise:

$$X_j(t) = \begin{cases} 1 & \text{if } t \in [t_{j-1}, t_j], \\ 0 & \text{otherwise.} \end{cases} \quad (3.2.15)$$

The Bernoulli trial  $X_j$  follows a binomial distribution  $B(1, P_{j,\Delta t})$ . Considering a sample of  $N_r$  rays, the variable  $Y_j = \sum_{k=1}^{N_r} X_j(t_k)$  follows a binomial distribution  $B(N_r, P_{j,\Delta t})$ , where  $t_k$  is the angle that the  $k$ -th ray forms with the optical axis. Then, using the de Moivre-Laplace theorem, we conclude that the variable  $Y_j$  is approximated by a normal distribution with mean value  $E[Y_j] = N_r P_{j,\Delta t}$  and variance  $\sigma^2[Y_j] = N_r P_{j,\Delta t}(1 - P_{j,\Delta t})$  when a large number of rays is considered, see [15, 16]. Thus, the normalized intensity along the direction  $t_{j-1/2}$  is

$$I_{MC}(t_{j-1/2}) = \sum_{k=1}^{N_r} X_j(t_k) / N_r. \quad (3.2.16)$$

The mean value  $E[I_{MC}(t_{j-1/2})] = P_{j,\Delta t}$  and the variance  $\sigma^2[I_{MC}(t_{j-1/2})] = P_{j,\Delta t}(1 - P_{j,\Delta t}) / N_r$ . Note that the standard deviation  $\sigma_j := \sigma[I_{MC}(t_{j-1/2})]$  equals

$$\sigma_j = \sqrt{P_{j,\Delta t}(1 - P_{j,\Delta t}) / N_r} = \frac{C_2}{\sqrt{N_b N_r}}, \quad (3.2.17)$$

for some  $C_2 > 0$ .  $\sigma_j$  can be used to give an estimate of the difference between the intensity  $I_{MC}(t_{j-1/2})$  and its mean value  $P_{j,\Delta t}$ . Therefore, the second term of the right hand side of relation (3.2.13) becomes

$$\begin{aligned} \frac{1}{\Delta t} \left| \int_{t_{j-1}}^{t_j} I(t) dt - \Phi I_{MC}(t_{j-1/2}) \right| &= \\ \frac{\Phi}{\Delta t} \left| P_{j,\Delta t} - I_{MC}(t_{j-1/2}) \right| &\propto \\ \frac{\Phi}{\Delta t} \sigma_j [I_{MC}(t_{j-1/2})] &= C_3 \frac{N_b}{\sqrt{N_b N_r}} = C_3 \sqrt{\frac{N_b}{N_r}}, \end{aligned} \quad (3.2.18)$$

for some  $C_3 > 0$ , where the approximation holds because  $\sigma_j$  gives a measure for the error between  $I_{MC}(t_{j-1/2})$  and the probability  $P_{j,\Delta t}$ , [17]. The second equality follows from Eq. (3.2.17). The MC error over the  $j$ -th bin is estimated by

$$\left| I(t_{j-1/2}) - \frac{\Phi}{\Delta t} I_{MC}(t_{j-1/2}) \right| = \frac{C_1}{N_b^2} + C_4 \sqrt{\frac{N_b}{N_r}}, \quad (3.2.19)$$

for  $C_4 > 0$ . Considering a fixed number of rays, we obtain that the minimal error is reached when  $N_b \approx N_r^{1/5}$ . Hence, if  $10^{10}$  rays are considered the target has to be

divided into  $10^2$  bins to minimize the MC error. This leads to computational efforts resulting in a very slow procedure.

We conclude this chapter implementing MC ray tracing for the two-faceted cup the profile of which is depicted in Fig. 3.1. Considering a set of  $N_r = 10^3$  random rays at the source, we obtain the distribution on the  $(x, t)$ -plane shown in Fig. 3.2.

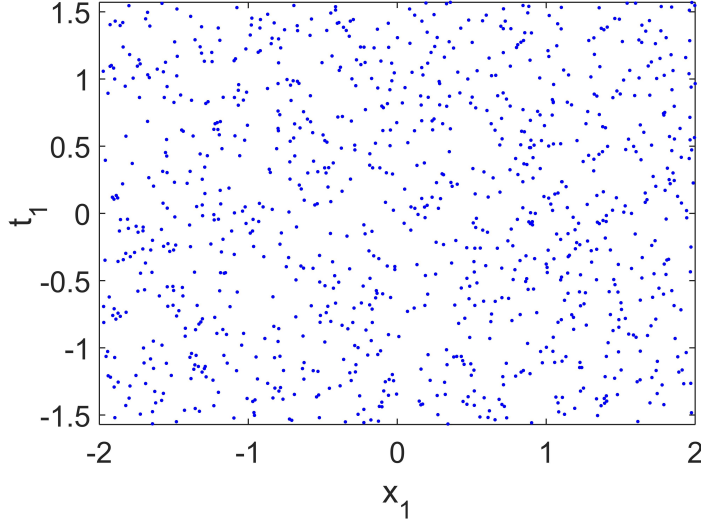


Figure 3.2: Rays at the source of the two-faceted cup with random position coordinate  $x$  and random angular coordinates  $t$ .  $10^3$  rays are depicted in this figure.

Then, every sample ray is traced inside the system using the ray tracing procedure. The target  $\mathbb{T} = [-b, b]$  is divided into  $N_b = 100$  bins. Using Eq. (3.2.10), the normalized intensity  $I_{MC}$  is computed.  $I_{MC}$  is a piecewise constant function, therefore the averaged normalized intensity  $\hat{I}_{MC}(t_{j-1/2}) = \frac{1}{\Delta t} I_{MC}(t_{j-1/2})$  is given considering the values that the intensity  $I_{MC}$  assumes on the middle point  $(t_{j-1/2})_{j=0, \dots, N_b}$  of every bin of the partitioning  $P_1$ . The profile of  $\hat{I}_{MC}$  is depicted in Fig. 3.3 with the red line. The exact intensity (analytic intensity) is shown with the green line in the same figure. MC ray tracing has the advantages of being very easy to implement and it does not require too much regularity of the function that has to be approximate. Furthermore, the error convergence does not depend on the dimension of the domain in which the function is defined. On the other hand, MC method is time consuming as the error, for a fixed number of bins, has a speed of convergence of order  $O(1/\sqrt{N_r})$ . Thus, to decrease the error of a factor 10 we need to increase the number of rays of a factor 100. As, MC ray tracing is a binning procedure, the error depends also on the number of bins in which the target is divided. It is a statistical procedure and the error bound is only a *probabilistic* error as shown in Eq. (3.2.9). This means that, to calculate the value of the error, several simulations have to be repeated and the average of the errors obtained in every simulation has to be calculated.

Instead of considering random variables, the sample of rays can be defined in such

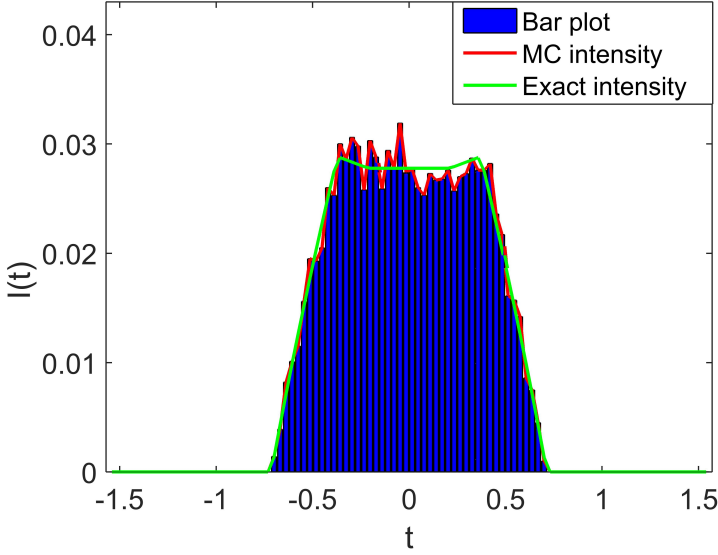


Figure 3.3: Comparison between the averaged normalized MC intensity and the normalized exact intensity.

a way that they have a regular distribution on the domain  $D \subseteq \mathbb{R}^d$  of the function  $f$  of which we want to compute the integral. Methods based on this deterministic approach are called Quasi Monte Carlo (QMC) methods. They can be seen as an improvement of MC method.

### 3.3 Quasi-Monte Carlo ray tracing

Quasi-Monte Carlo (QMC) methods were proposed for the first time in the 1950s in order to deal with the issues encountered in MC. Likewise MC methods, QMC procedures can be used to approximate the integral of a function. It is useful to restrict ourselves to intervals of the form  $[\mathbf{a}, \mathbf{b}] \subseteq [0, 1]^d$  and introduce the concept of sequences uniformly distributed modulo one.

**Definition 3.3.1.** An infinite sequence  $\{y_n\}_{n \in \mathbb{N}_0} \in [0, 1]^d$  is said to be *uniformly distributed modulo one* (or *equidistributed*), if for every interval  $[\mathbf{a}, \mathbf{b}] \subseteq [0, 1]^d$  it holds

$$\lim_{N \rightarrow \infty} \frac{\text{card}(A([\mathbf{a}, \mathbf{b}], N))}{N} = \lambda_d([\mathbf{a}, \mathbf{b}]) \quad (3.3.1)$$

where  $\text{card}(A([\mathbf{a}, \mathbf{b}], N))$  is the cardinality of the following set

$$A([\mathbf{a}, \mathbf{b}], N) = \{n \in \mathbb{N}_0 : 0 \leq n \leq N - 1 \text{ and } y_n \in [\mathbf{a}, \mathbf{b}]\}, \quad (3.3.2)$$

and  $\lambda_d([\mathbf{a}, \mathbf{b}]) = \prod_{j=1}^d (b_j - a_j)$  is the  $d$ -dimensional Lebesgue measure of the interval  $[\mathbf{a}, \mathbf{b}]$ .



Given a sequence  $\{\mathbf{y}_i\}_{i=1, \dots, N} \in [0, 1)^d$  uniformly distributed modulo one and a Riemann integrable function  $f : [0, 1]^d \mapsto \mathbb{R}$ , the integral of  $f$  can be approximate as the average of the values that  $f$  assumes on  $\{\mathbf{y}_i\}$  for every  $j = \{1, \dots, N\}$ , that is:

$$\lim_{N \rightarrow \infty} \frac{1}{N} \sum_{i=1}^N f(\mathbf{y}_i) = \int_{[0,1]^d} f(\mathbf{y}) d\mathbf{y}. \quad (3.3.3)$$

The idea of QMC methods is to generate the set of points in  $[\mathbf{a}, \mathbf{b}]$  such that they are not random distributed but also not exactly uniformly distributed. To measure how much the distribution of these points differs from a uniform distribution, the concept of discrepancy was introduced. Intuitively, discrepancy measures how much the samples differ from a uniform distribution. Therefore, random sequences have a very high discrepancy, while uniform distributed sequences have zero discrepancy. The definition of discrepancy in more mathematical terms is provided below.

**Definition 3.3.2.** Given a set  $\mathcal{S} = \{\mathbf{y}_1, \dots, \mathbf{y}_N\}$  of  $N$  points in  $[0, 1)^d$ . The discrepancy  $D_N(\mathcal{S})$  of  $\mathcal{S}$  is defined as

$$D_N(\mathcal{S}) = \sup_{\mathbf{a}, \mathbf{b} \in [0,1]^d} \left| \frac{\text{card}(A([\mathbf{a}, \mathbf{b}], N))}{N} - \lambda_d([\mathbf{a}, \mathbf{b}]) \right| \quad (3.3.4)$$

where  $\lambda_d([\mathbf{a}, \mathbf{b}]) = \prod_{j=1}^d (b_j - a_j)$  is the  $d$ -dimensional Lebesgue measure of the interval  $[\mathbf{a}, \mathbf{b}]$ .

Often, it is enough to consider the discrepancy in the intervals  $[0, \mathbf{a}] \subseteq [0, 1)^d$ , in that case we talk about star discrepancy.

**Definition 3.3.3.** Let  $\mathcal{S} = \{\mathbf{y}_1, \dots, \mathbf{y}_N\}$  be a set of  $N$  points in  $[0, 1)^d$ . The star discrepancy  $D_N^*(\mathcal{S})$  of  $\mathcal{S}$  is defined as:

$$D_N^*(\mathcal{S}) = \sup_{\mathbf{a} \in [0,1]^d} \left| \frac{\text{card}(A([0, \mathbf{b}], N))}{N} - \lambda_d([0, \mathbf{a}]) \right| \quad (3.3.5)$$

Sequences constructed such that the corresponding star discrepancy has an order of  $O(\log(N)^d/N)$  are called *low-discrepancy sequences*, [13]. An important results shows that, using a low-discrepancy sequence  $\{\mathbf{y}_i\}_{i=1, \dots, N}$ , the absolute error of a QMC algorithm:

$$\text{err}(f, S_N) = \left| \int_{[0,1]^d} f(\mathbf{y}) d\mathbf{y} - \frac{1}{N} \sum_{i=1}^N f(\mathbf{y}_i) \right| \quad (3.3.6)$$

can be bounded by the product of a term that depends on  $f$  and another term that depends on the discrepancy of the set  $\{\mathbf{y}_i\}_{i=1, \dots, N}$ . This is the result provided by the Koksma-Hlawka inequality which gives the following estimation of the error:

$$\left| \int_{[0,1]^d} f(\mathbf{y}) d\mathbf{y} - \frac{1}{N} \sum_{i=1}^N f(\mathbf{y}_i) \right| \leq V(f) D_N^*(\mathcal{S}) \quad (3.3.7)$$

where  $V(f)$  is the so-called variation function of  $f$  in the sense of Hardy-Krause (see [18, 19] for details). From the definition of low-discrepancy sequences and from the

Koksma-Hlawka inequality we can state that:

$$\text{err}(f, S_N) < C \frac{\log(N)^d}{N}. \quad (3.3.8)$$

For small dimensions  $d$ , QMC performs much better than MC methods, while for large dimension  $d$  the factor  $\log(N)$  could be very big. The convergence of QMC method can depend on which kind of low-discrepancy sequence is used. Indeed, there are many ways to generate such sequences. The most common QMC approach uses the so-called Sobol' sequence. The algorithm for generating Sobol' sequences is widely explained in the literature, (see for instance, [20]). In appendix A we give an overview of how these kind of sequences can be constructed.

Based on QMC methods, QMC ray tracing considers as position and angular coordinates of the rays at the source, the coordinates of the corresponding points of a low-discrepancy sequence. Therefore, to implement QMC ray tracing in two-dimensions we need to construct a low-discrepancy sequence in two-dimensions. Given, for instance, a Sobol' sequence  $\{\mathbf{y}_i\}_{i=1,\dots,N}$  with  $\mathbf{y}_i \in [0, 1]^2$  for every  $i = 1, \dots, N$ , the two dimensional QMC ray tracing consider the position coordinate of the  $i$ -th ray at the source equal to the first component of the  $i$ -th point  $\mathbf{y}_i$  of the Sobol' sequence  $\{\mathbf{y}_i\}_{i=1,\dots,N}$  and, the direction coordinate of the  $i$ -th ray at the source equal to the second component of the  $i$ -th point  $\mathbf{y}_i$  of the same sequence. A set of  $N_r = N$  rays with these initial coordinates is traced within the system and, once the target coordinates of all the rays traced are computed, the output intensity is calculated using the same approach used for MC ray tracing, see Eqs 3.2.10 and 3.2.13. The difference between MC and QMC ray tracing consists only on the choice of the initial ray set.

In Fig. 3.4 we show the distribution of the position and direction coordinates of the rays at the source of the two-faceted cup in Fig. 3.1. A set of  $10^3$  rays generated from a 2D Sobol sequence is considered, the coordinates  $(x_1, t_1)$  of every ray at the source are depicted with blue dots. We note that the rays have a regular distribution on the  $(x, t)$ -plane. We need to remark that, for the system in Fig. 3.1,  $x_1 \in [-2, 2]$  and the angular coordinates  $t_1 \in [-\pi/2, \pi/2]$ . Since Sobol' sequences are defined inside intervals of the  $[\mathbf{a}, \mathbf{b}] \subseteq [0, 1]^2$ , we scaled the points of the sequence  $\mathbf{y}_i$  in order to take all the possible positions and directions that the rays can assume at the source.

Dividing the target into  $N_b = 100$  bins, we computed the target intensity. In Fig. 3.5 we show the profile of the output intensity at the target of the two-faceted cup computed using QMC ray tracing with  $10^4$  rays. The QMC intensity is depicted with the red line. It is compared to the analytic intensity shown in the same figure with the green dotted line. A comparison between Fig. 3.3 and 3.5 gives the insight that for the two-faceted cup and for a set of  $N_r = 10^4$  rays, QMC ray tracing performs better than MC ray tracing. In order to show the accuracy obtained using MC and QMC methods, we calculate the target intensity gradually increasing the number of rays traced inside the two-faceted cup. The error between the approximate intensity and the analytic intensity is calculated for every sample of rays. The speed of convergence for MC is shown in Fig. 3.6 with the red, while the behavior of QMC ray tracing is depicted in the same picture with the blue line. The results shown for a simple optical system are indeed consistent with what we expected from the theoretical analysis. Although QMC ray tracing is an improvement of MC ray tracing for small dimensions, it has two main disadvantages. First, its convergence is strongly related with the

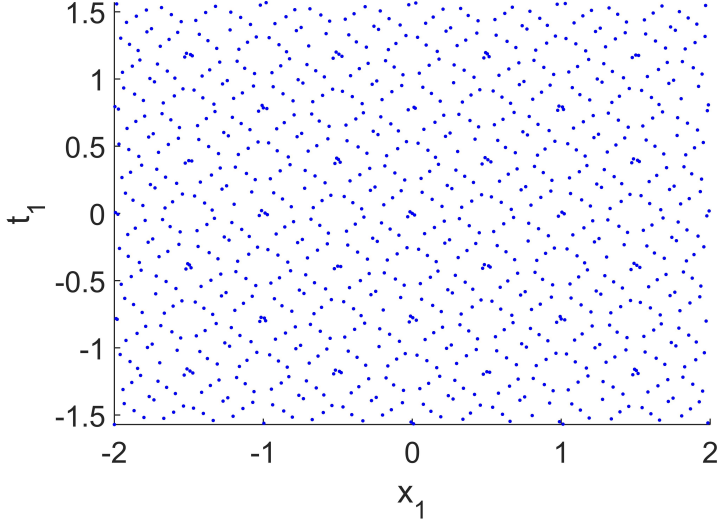


Figure 3.4:  $10^3$  rays at the source of the two-faceted cup with position  $x_1$  and angular  $t_1$  coordinates with a regular distributions. They are distributed as the points of a Sobol' sequence in two-dimensions.

dimension in which it is implemented. Second, likewise MC ray tracing, QMC ray tracing is a binning procedure, therefore the error still depends on the number of bins in which the target is divided and only the averaged value of the intensity over every bin is provided.

From the results provided in this chapter we can conclude that the choice of the initial ray set can make a big impact on the performance of the ray tracing procedure. Based on the idea of taking a smart choice of the initial ray set, we develop a new ray tracing method which is based on phase space. The phase space (PS) concept will be introduced in the next chapter. The new ray tracing method employs the PS of the source and the target of the optical systems. We will show in this thesis that phase space ray tracing allows to trace only few rays inside the system to obtain the desired accuracy of the target intensity.

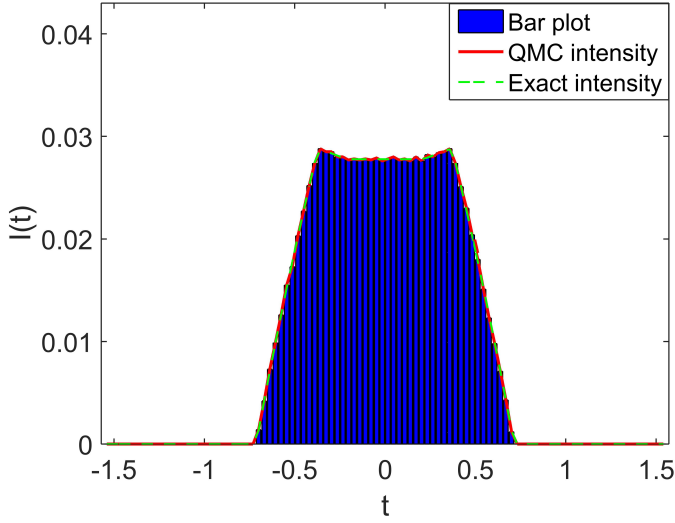


Figure 3.5: QMC intensity for the two-faceted cup obtained tracing  $N_r = 10^4$  rays and dividing the target into  $N_b = 100$  bins.

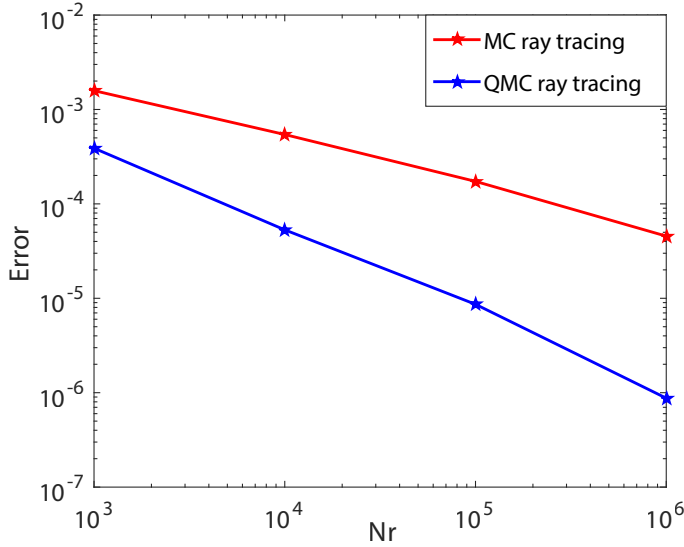


Figure 3.6: Error as function of the number of rays traced in a logarithmic scale for fixed number of bins  $N_b = 100$ . MC ray tracing convergence is of the order  $O(1/\sqrt{N_r})$  and it is shown with the red line. QMC ray tracing convergence is of the order  $O(1/N_r)$  and it is depicted with the blue line.

## Chapter 4

# Ray tracing on phase space

### 4.1 Phase space concept

The PS of a three-dimensional systems is a four-dimensional space since every ray is described by two position coordinates and two direction coordinates. The two position coordinates are given by two of the coordinates of the intersection point of the ray with the surface, while the two direction coordinates are the momentum coordinates of the vector tangent to the ray projected on the optical surface, see [21].

For two-dimensional systems every ray in the PS of a line is given by a point in a two-dimensional space. The position coordinate in the PS of line  $j$  is the  $x$ -coordinate of the intersection point between the ray and line  $j$ . The direction coordinate is the sine of the angle that the ray forms with respect to the normal of line  $j$  multiplied by the index of refraction of the medium in which the ray is located. We indicate the PS with  $S=Q \times P$ , where  $Q$  is the set of the position coordinates  $q$  and  $P$  is the set of the direction coordinates  $p = n \sin \theta$  with  $\theta$  the angle between the ray and the normal  $\boldsymbol{\nu}$  of the line and  $n$  is the index of refraction of the medium in which the line is located. The normal  $\boldsymbol{\nu}$  is always directed inside the same medium in which the incident ray travels and, the angle  $\theta$  between the ray and  $\boldsymbol{\nu}$  is measured counterclockwise. In the following, the phase space is considered only for the source  $S$  and the target  $T$  and for no other line of the optical system. The coordinates of every ray in  $S$  and  $T$  PS are indicated with  $(p_1, q_1)$  and  $(p, q)$ , respectively.

The source and target phase spaces are partitioned into different regions according to the path  $\Pi$  followed by the rays. Given a path  $\Pi$ , the corresponding regions are indicated with  $R_1(\Pi)$  and  $R(\Pi)$  at the source and the target PS, respectively. Ries and Rabl (1994) showed that the boundaries  $\partial R_1(\Pi)$  at the source are mapped into the boundaries  $\partial R(\Pi)$  at the target: all rays that are neighbors at the source PS remain close to each other at the target PS, [22].

Using the PS concept and the edge-ray principle, we develop a new ray tracing procedure in PS. The idea is to construct a nonuniform triangulation on PS in such a way that new triangles are added only where boundaries occur.

## 4.2 Phase space ray tracing

The regions  $(R_{t,\Pi_j})_{j=1,\dots,p}$  can be defined only when some rays are traced. Given an initial set of rays, the rays closest to the boundaries  $(\partial R_{t,\Pi_j})_{j=1,\dots,p}$  are selected and more rays in their vicinity are created to get progressively better estimates of the boundaries. A more detailed description is provided below. A triangulation in  $\mathcal{P}_s$  is defined and a ray from every vertex  $(x_k, \tau_k)$  of the triangle is traced. The procedure starts tracing four rays with coordinates  $(x_k, \tau_k)_{k=1,\dots,4}$  that are located exactly at the corners of  $\mathcal{P}_s$  and, for each of them, the paths  $(\Pi_j)_{j=1,\dots,4}$ , are stored. Next, for some  $j \in \{1, \dots, 4\}$ , the grid is divided into two equal triangles joining two opposite vertices. For each triangle the rays located at its corners are traced. If the paths corresponding to those rays are different, one or more boundaries  $(\partial R_{t,\Pi_j})_{j=1,\dots,4}$  are expected to cross the triangle. In that case, the middle points  $(x_k, \tau_k)_{k=5,6,7}$  of each side of the triangle are added and three more rays with coordinates  $(x_k, \tau_k)_{k=5,6,7}$  are traced. Each refinement step leads to four new triangles (see Figure 4.1).

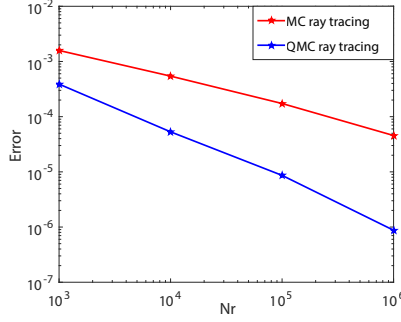


Figure 4.1: Triangulation refinement: when the rays related to the vertices of the triangles follow a different path a new refinement step is required. Each refinement step leads to four new triangles. The parameters values are  $\epsilon_{x_{max}} = 2$ ,  $\epsilon_{\tau_{max}} = 1$ ,  $\epsilon_{x_{min}} = 4$  and  $\epsilon_{\tau_{min}} = 2$ .

When all the rays in the corners of each triangle have the same path, it is not necessary to refine the triangles anymore. Note that it can happen that a region formed by rays that follow a path  $\Pi_j$  is located completely inside a triangle whose vertices are related to the same path  $\Pi_i$  with  $j \neq i$ . In that case the algorithm is not able to detect that region, see Figure 4.2. To avoid this, two parameters  $\epsilon_{x_{min}}$  and  $\epsilon_{\tau_{min}}$  are defined for the  $x$ -axis and the  $\tau$ -axis, respectively. When the length of the sides of the triangle are greater than these parameters, a new triangle is defined even if its vertices correspond to the same path. Furthermore, two other parameters  $\epsilon_{x_{max}}$  and  $\epsilon_{\tau_{max}}$  are introduced to define a stopping criterion. The algorithm stops when the length of the sides of the triangles is smaller than  $\epsilon_{x_{max}}$  and  $\epsilon_{\tau_{max}}$ . The values of the parameters  $\epsilon_{x_{max}}$ ,  $\epsilon_{\tau_{max}}$ ,  $\epsilon_{x_{min}}$  and  $\epsilon_{\tau_{min}}$  determine the number of rays traced. Indeed, on the one hand,  $\epsilon_{x_{max}}$  and  $\epsilon_{\tau_{max}}$  can be decreased to obtain more rays close to the boundaries; on the other hand, a large number of rays in the interior of the regions can be traced decreasing the values of  $\epsilon_{x_{min}}$  and  $\epsilon_{\tau_{min}}$ .

Using the above procedure, rays increasingly closer to the boundaries are traced. For our optical system, the width of the  $x$ -axis in source phase space is two times the

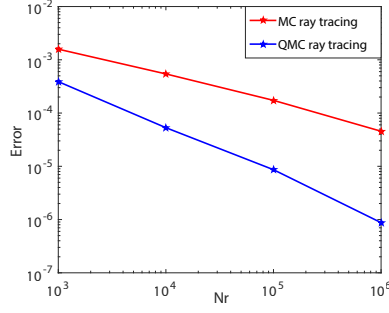


Figure 4.2: The red line encloses a region of rays that follow the path  $\Pi_2$  and is completely located inside a triangle. The algorithm is not able to detect that region and, a further refinement is required. The parameters values are  $\epsilon_{x_{max}} = 2$ ,  $\epsilon_{\tau_{max}} = 1$ ,  $\epsilon_{x_{min}} = 4$  and  $\epsilon_{\tau_{min}} = 2$ .

width of the  $\tau$ -axis. Thus, our choice is  $\epsilon_{\tau_{min}} = \frac{1}{2}\epsilon_{x_{min}}$  and  $\epsilon_{\tau_{max}} = \frac{1}{2}\epsilon_{x_{max}}$ . Figure 4.3 shows an example of a triangulation refinement of the source phase space with  $\epsilon_{x_{max}} = 0.1$  and  $\epsilon_{x_{min}} = 1$ . The triangulation refinement provides more triangles close to the boundaries  $\partial R_{s,\Pi_j}$  than those inside the regions  $R_{s,\Pi_j}$ .

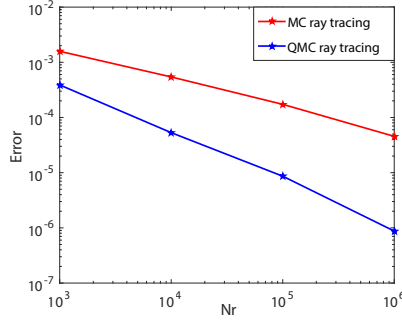


Figure 4.3: Triangulation refinement of source phase space: near the boundaries more rays are traced. The values of the parameters are  $\epsilon_{x_{max}} = 0.1$  and  $\epsilon_{x_{min}} = 1$ .

The paths  $(\Pi_j)_{j=1,\dots,p}$  followed by the rays located at the corner of the triangles are computed during the procedure and, the regions  $R_{s,\Pi_j}$  and  $R_{t,\Pi_j}$  are defined for each  $\Pi_j$ . Next, a criterion to select the values of the parameters  $\epsilon_{x_{min}}$  and  $\epsilon_{x_{max}}$  and a method to compute the boundaries  $\partial R_{t,\Pi_j}$  is provided. Furthermore, the output photometric variables are computed, the details are explained in the next section.

A similar method as described here is presented by Moore, [?]. In Moore's method each ray leaves the source at the same position while the angle coordinate changes. The path followed by the rays is taken into account and an interpolation is required to finalize the illumination pattern. This interpolation can affect the efficiency of the method. Our method employs the distribution of the rays at the target phase space and avoids using any interpolation. Moreover, a criterion to stop the algorithm is

provided in such a way that no more rays than necessary are traced. This makes ray tracing in phase space more accurate compared with Moore's procedure. Finally, we claim that PS ray tracing is also more accurate than the ray tracing procedure proposed by Moore (2013), [?]. The novelty of our approach compared to the method used by Moore, is briefly explained below. First, to compute the output intensity, we employ the phase space of the target. This avoids the use of any interpolation to compute the photometric variables and therefore, more accurate results are obtained. Second, in [?] all rays that leave the source start at the same position and only a sampling angular range is given. In our approach a rectangular source is considered thus, both the angular and spatial coordinates of each ray change. This extra variable can produce very irregular shapes of the regions at target phase space. To overcome this issue, we employ the edge-ray principle and we consider the regions at source phase space where the distribution of the rays is much more regular and the corresponding boundaries are easily computed. As a consequence, our procedure is suitable to compute the output intensity as function of both the angular or the spatial coordinates.

### 4.3 Comparison between MC, QMC and PS ray tracing



## Chapter 5

# Two different approaches to compute the boundaries in target phase space

5.1 The  $\alpha$ -shapes approach

5.2 The two-faceted cup

5.3 Results for a TIR collimator

5.4 The triangulation refinement approach

5.5 The two-faceted cup

5.6 Results for a TIR collimator

5.7 Results for a Parabolic reflector

5.8 Results for the Compound Parabolic Concentrator (CPC)



## Chapter 6

# The inverse ray mapping method: analytic approach

6.1 Explanation of the method

6.2 The two-faceted cup

6.3 Results for the two-faceted cup

6.4 Results for the multi-faceted cup

6.5 Discussions



## Chapter 7

# The extended ray mapping method

7.1 Explanation of the method

7.2 Bisection procedure

7.3 Results for a parabolic reflector

7.4 Results for two different kind of TIR-collimators



## Chapter 8

# Extended ray mapping method to systems with Fresnel reflection





## Chapter 9

# Discussion and conclusions



# Appendix A

## Implementation of Sobol' sequences

### A.1 Van der Corput sequences

In the following we show a particular construction of a low-discrepancy sequence for  $d = 1$  that was introduced the first time by Van der Corput in 1935. This kind of sequences, called *van der Corput* sequences, are particular interesting not only because they give an intuition of how to construct low discrepancy sequences but also because many other kind of sequences in higher dimensions are based on this one-dimensional case. Before introducing these sequences we need to give the concept of radical inverse function. Let  $b \geq 2$  be an integer base. Any natural number  $n \in \mathbb{N}_0$  can be decomposed in base  $b$  as follows:

$$n = \sum_{i=0}^{\infty} d_i b^i \quad (\text{A.1.1})$$

where  $d_i \in \{0, 1, \dots, b-1\}$  are the digit numbers. The radical inverse function  $\phi_b : \mathbb{N}_0 \mapsto [0, 1)$  in base  $b$  is defined as:

$$\phi_b(n) = \sum_{i=1}^{\infty} \frac{d_{i-1}}{b^i}. \quad (\text{A.1.2})$$

As an example we provide in the following the radical inverse function  $\phi_b(5)$  in base  $b = 2$ . The digit expansion in base  $b$  of  $n = 5$  is:

$$5 = 1 \cdot 2^0 + 1 \cdot 2^2. \quad (\text{A.1.3})$$

Therefore,  $d_0 = 1, d_1 = 0$  and  $d_2 = 1$ . The radical inverse function  $\phi_2(5)$  is:

$$\phi_2(5) = \frac{1}{2} + \frac{1}{8} = \frac{5}{8}. \quad (\text{A.1.4})$$

**Definition A.1.1.** The Van der Corput sequence in base  $b$  is defined as  $\{\phi_b(n)\}_{n \in \mathbb{N}_0}$ .

For example, suppose we have the finite sequence of numbers  $n \in \{0, 1, \dots, 8\}$  the corresponding Van der Corput sequence  $\{\phi_b(n)\}_{n \in \{0, 1, \dots, 8\}}$  in base  $b = 2$  is:

$$\{\phi_2(n)\}_{n \in \{0, 1, \dots, 8\}} = \left\{0, \frac{1}{2}, \frac{1}{4}, \frac{3}{4}, \frac{1}{8}, \frac{5}{8}, \frac{3}{8}, \frac{7}{8}, \frac{1}{16}\right\}. \quad (\text{A.1.5})$$

It can be proved that the Van der Corput sequence in base  $b$  is uniformly distributed modulo one, [14]. The van der Corput sequence has been extended to higher dimensions. The most common QMC approach uses Sobol sequence which can be seen as an extended Van der Corput sequence in base  $b = 2$ . Sobol' sequence uses the same base  $b = 2$  for all the dimensions  $d \geq 2$ .

## A.2 Sobol' sequences

The aim is to generate a low-discrepancy sequence in the ipercube  $[0, 1]^d$ . Let us start from the simplest case of one dimension, i.e.  $d = 1$ . First, we need to chose a primitive polynomial  $P_j$  of degree  $s_j$  of the form

$$P_j : x^{s_j} + a_{1,j}x^{s_j-1} + \dots + a_{s_j-1,j}x + 1 \quad (\text{A.2.1})$$

where the coefficients  $\{a_{i,j}\}_{i=1, \dots, s_j-1}$  are either 0 or 1. Then a sequence  $\{m_1, m_2, \dots\}$  is defined such that:

$$m_{k,j} := 2a_{1,j}m_{k-1,j} \oplus 2^2a_{2,j}m_{k-2,j} \oplus \dots \oplus 2^{s-1}a_{k-1,j}m_{k-s+1,j} \oplus 2^s m_{k-1,j} \oplus m_{k-s,j}, \quad (\text{A.2.2})$$

where we have indicated with  $\oplus$  the bit by bit exclusive or operator which operates on two bit patterns and operates on each pair of the corresponding bins giving as result 1 if one of the two bits is 1 and 0 if both bits are equal either to 0 or 1. The values  $m_{k,j}$ ,  $1 \leq k \leq d$ , are chosen such that they are odd and positive numbers less than  $2^k$ . Now, the so-called direction numbers are defined by:

$$v_{k,j} = \frac{m_{k,j}}{2^k}. \quad (\text{A.2.3})$$

Then, the sequence  $\{x_{i,j}\}$  is given by

$$x_{i,j} = i_1 v_1 \oplus i_2 v_2 \oplus \dots \quad (\text{A.2.4})$$

for every  $i$ , where  $i_k$  is the  $k$ -th digit from the right when  $i$  is written in binary  $i = (\dots i_3 i_2 i_1)_2$ , [23]. We provide in the following an example.

Given the primitive polynomial  $x^3 + x^2 + 1$  of degree  $s_j = 3$ , the first three coefficients  $m_{1,j} = 1$ ,  $m_{2,j} = 3$ , and  $m_{3,j} = 7$  lead to the following direction numbers

$$v_{1,j} = \frac{1}{2}, \quad v_{2,j} = \frac{3}{4}, \quad v_{3,j} = \frac{7}{8}, \quad (\text{A.2.5})$$

that in binary notation are:

$$v_{1,j} = (0.1)_2 \quad v_{2,j} = (0.11)_2, \quad v_{3,j} = (0.111)_2. \quad (\text{A.2.6})$$

From Eq. (A.2.2) we can derive the others coefficients  $m_{4,j} = 5$ ,  $m_{5,j} = 7$ , etc. with the corresponding direction vectors:

$$v_{4,j} = \frac{5}{16} = (0.0101)_2 \quad v_{5,j} = \frac{7}{32} = (0.00111)_2 \quad (\text{A.2.7})$$

From Eq. (A.2.4) we finally find the sequence

$$(\text{A.2.8})$$

The generalization of Sobol's sequence to higher dimensions  $d > 1$  is calculated considering a sequence where the  $i$ -th point has the form:

$$q_i = (x_{i,1}, x_{i,2} \dots, x_{i,d}), \quad (\text{A.2.9})$$

where the second index of the variables  $x_{i,j}$  it refers to the polynomial  $P_j$  (with corresponding degree  $s_j$ ) which is considered to calculate the direction numbers. Therefore,  $d$  different sets of direction numbers are generated from a given polynomial  $P_j$  using Eq. A.2.3 and each component  $x_{i,j}$  is computed using the corresponding direction vector.



# Description of the research

In this thesis we studied the light propagation within optical systems. Optical engineers are interested in design systems in such a way the desired output distribution is obtained. The goal in illumination optics is to obtain the desired output distribution of light. To this purpose the ray tracing procedure is widely used. Ray tracing is a forward method where a set of rays is traced within the system from the source to the target. The propagation of light is determined computing the position and the direction of every ray for all the optical surfaces that it encounters. There are many ways to implement the ray tracing process. Monte Carlo (MC) ray tracing is often used in non-imaging optics. Rays are randomly traced from the source to the target and each time that a ray hits an optical surface the coordinates of the intersection point of the ray with the surface and the new ray direction are calculated. The output variables are computed dividing the target into intervals, the so-called bins, and counting the rays that fall into each bin. To obtain the desired accuracy, millions of rays are required, therefore the method is extremely computationally expensive and it converges as the inverse of the square root of the number of rays traced.

MC ray tracing can be improved using as sample of points a low discrepancy sequence instead of random points. Discrepancy can be interpreted as a measure of how much the sample distribution differs from a uniformly distributed sample. The discrepancy is therefore zero for uniformly distributed points. A low discrepancy sequence gives a sample of points which are regularly distributed but not exactly uniformly distributed. Quasi Monte Carlo (QMC) method considers these kind of sequences as sample of points. Therefore, QMC ray tracing is implemented tracing a set of rays whose position and direction are given by the coordinates of a low discrepancy sequence of points. The main advantage of QMC method is its rate of convergence, it is faster than MC for low dimensional problems. Nevertheless, it has some disadvantages. First, it is not easy to give an error estimation for QMC method. Second, for high dimensional spaces the QMC can become very slow. Third, it is still a binning procedure. Hence, the accuracy depends both on the number of rays traced and on the number of bins.

In order to improve the existing methods, the phase space (PS) of the optical system is considered in this thesis. The PS of an optical surface gives information about the position and the direction of every ray on that surface where the direction is expressed with respect to the normal of the surface. In PS, the ray's direction is given by the sine of the angle that the ray forms with respect to the normal of the surface multiplied by the index of refraction of the medium in which the ray is located. In two dimensions, the PS is a two-dimensional space where the coordinates of every

ray are specified by one position coordinate and one angular coordinate. For three dimensional systems the PS is a four dimensional space because every ray is specified by two position and two angular coordinates. Our idea is to use the structure of PS to trace only the rays close to the discontinuities of the luminance at the target PS. Two new approaches based on PS are presented in this work. They are tested for two-dimensional systems.

The first method is called ray tracing on PS and it is based on the source and the target PS representation of the optical system. It takes into account the sequence of optical lines that each ray hits when it propagates inside the system, that is the ray path. We note that the source and target phase spaces are partitioned into different regions each of them is formed by the rays that follow the same path. The idea is to use the edge-ray principle proved by Ries and Rabl (1994) which states that the area of these regions is conserved: all rays that are neighbors at the source PS remain close to each other at the target PS. To this purpose, a nonuniform triangulation of the source PS is constructed in such a way that new triangles are added to the triangulation only where boundaries occur. Assuming constant brightness, we only need to compute the boundaries of the regions in target PS to obtain the output photometric variables. We test the method for optical systems where both reflection and refraction laws are involved. Numerical results show that ray tracing on PS is faster and more accurate compared to MC ray tracing.

The second method employs not only the source and the target PS, but also the PS of *all* the other lines that constitute the system. All lines can be modeled as detectors of the incident light and emitters of the reflected light. Moreover, we assume that the source can only emit light and the target can only receive light. Therefore, one PS is taken into account for the source and one for the target. For the other surfaces both the source and target PS are considered. Furthermore, instead of starting from the source, the new method starts tracing back rays from target PS. In order to determine the coordinates of these rays, an inverse map from the target to the source PS is constructed as a concatenation of the maps that relate the PS of two different lines. Employing this map we are able to detect the rays that in target PS are located on the boundaries of the regions with positive luminance. First, we implement the method for systems formed by straight and reflective lines. In this particular case, the boundaries of the regions that form every PS can be computed analytically. This allows us to obtain an analytic target intensity distribution. The results are shown for a two-faceted cup and a multi-faceted cup. In both cases we note significant advantages both in terms of the accuracy and the computational time. Second, the method is developed for systems formed by curved lines. In this case the boundaries cannot be determined analytically and therefore a numerical procedure is involved. In particular, we apply a bisection method on target PS. Also in this case we compare our method to MC ray tracing and we observe significant advantages using the PS method. Finally, the ray mapping method in PS is applied to systems where also Fresnel reflection is taken into account. We obtain relevant results also in the last case.



# Curriculum Vitae

Carmela Filosa was born on November 28, 1985 in Torre del greco, Italy. She finished the high school in 2003 at Liceo Scientifico Statale "G. Marconi", Colleferro. She obtained a bachelor (2008) and Master (2013) degree in Mathematics at the University of Rome "La Sapienza", Italy. In March 2014, she moved in Eindhoven (the Netherlands) to start a PhD project at the Eindhoven University of Technology in the department of Mathematics and Computer Science. The PhD project was under the supervision of Wilbert IJzerman and Jan ten Thije Boonkkamp. The research conducted in her doctoral studies was funded by Technologiestichting STW and, the daily work took place at the Centre for Analysis, Scientific computing and Applications (CASA) of TU/e and at the department of Philips Lighting of the High Tech Campus in Eindhoven. The results of her research are presented in this thesis.



# Acknowledgments



# Bibliography

- [1] E. F. Zalewski, “Radiometry and photometry,” *Handbook of optics*, vol. 2, pp. 24–1, 1995.
- [2] J. Chaves, *Introduction to nonimaging optics*. CRC press, 2015.
- [3] “Luminous efficacy-wikipedia the free encyclopedia,” [https://commons.wikimedia.org/wiki/File:CIE\\_1931\\_Luminosity.png](https://commons.wikimedia.org/wiki/File:CIE_1931_Luminosity.png) *media/File:CIE\_1931\_Luminosity.png*.
- [4] A. V. Arecchi, R. J. Koschel, and T. Messadi, “Field guide to illumination,” SPIE, 2007.
- [5] H. Zhu and P. Blackborow, “Etendue and optical throughput calculations,” *Energetiq Technology, Inc., Woburn, MA*, 2011.
- [6] R. P. Feynman, “Feynman lectures on physics. volume 2: Mainly electromagnetism and matter,” *Reading, Ma.: Addison-Wesley, 1964, edited by Feynman, Richard P.; Leighton, Robert B.; Sands, Matthew*, 1964.
- [7] M. Born and E. Wolf, *Principles of optics: electromagnetic theory of propagation, interference and diffraction of light*. Elsevier, 2013.
- [8] E. Hecht, *Optics*. Parson Addison-Wesley, 2002.
- [9] R. P. Feynman, R. B. Leighton, and M. Sands, *The Feynman lectures on physics, Vol. I: The new millennium edition: mainly mechanics, radiation, and heat*, vol. 1. Basic books, 2011.
- [10] P. H. Jones, O. M. Maragò, and G. Volpe, *Optical tweezers: Principles and applications*. Cambridge University Press, 2015.
- [11] R. Winston, J. C. Miñano, and P. Benitez, *Nonimaging optics*. Academic Press, 2005.
- [12] H. Gross, *Handbook of the Optical Systems*, vol. 1. Wiley-VCH, 2005.
- [13] A. B. Owen, “Quasi-monte carlo sampling,” *Monte Carlo Ray Tracing: Siggraph*, vol. 1, pp. 69–88, 2003.
- [14] G. Leobacher and F. Pillichshammer, *Introduction to quasi-Monte Carlo integration and applications*. Springer, 2014.

- [15] V. M. Zolotarev, *Modern theory of summation of random variables*. Walter de Gruyter, 1997.
- [16] R. Y. Rubinstein and D. P. Kroese, *Simulation and the Monte Carlo method*, vol. 10. John Wiley & Sons, 2016.
- [17] D. M. Diez, C. D. Barr, and M. Cetinkaya-Rundel, *OpenIntro statistics*. CreateSpace, 2012.
- [18] L. Brandolini, L. Colzani, G. Gigante, and G. Travaglini, “A koksma–hlawka inequality for simplices,” in *Trends in harmonic analysis*, pp. 33–46, Springer, 2013.
- [19] A. B. Owen, “Multidimensional variation for quasi-monte carlo,” in *International Conference on Statistics in honour of Professor Kai-Tai Fang’s 65th birthday*, pp. 49–74, 2005.
- [20] P. Bratley and B. L. Fox, “Algorithm 659: Implementing sobol’s quasirandom sequence generator,” *ACM Transactions on Mathematical Software (TOMS)*, vol. 14, no. 1, pp. 88–100, 1988.
- [21] K. B. Wolf, *Geometric optics on phase space*. Springer Science & Business Media, 2004.
- [22] H. Ries and A. Rabl, “Edge-ray principle of nonimaging optics,” *JOSA A*, vol. 11, no. 10, pp. 2627–2632, 1994.
- [23] S. Joe and F. Y. Kuo, “Notes on generating sobol sequences,” *ACM Transactions on Mathematical Software (TOMS)*, 29 (1), 49, vol. 57, 2008.